Article

Characteristics of Recent Aftershocks Sequences (2014, 2015, 2018) Derived from New Seismological and Geodetic Data on the Ionian Islands, Greece

Alexandra Moshou [1,*] , **Panagiotis Argyrakis** [1] , **Antonios Konstantaras** [2] , **Anna-Christina Daverona** [3] **and Nikos C. Sagias** [4]

1   Institute of Geodynamics, National Observatory of Athens, Lofos Nymphon, 11810 Athens, Greece; pargyrak@noa.gr

2   Department of Electronic Engineering, Hellenic Mediterranean University, 3 Romanou Str., Chalepa, 73133 Chania, Crete, Greece; akonstantaras@hmu.gr

3   Department of Surveying and Geoinformatics Engineers, Faculty of Engineering, Egaleo Park Campus, University of West Attica, Ag. Spyridonos Street, Aigaleo, 12243 Athens, Greece; adaverona@uniwa.gr

4   Department Informatics and Telecommunications, Faculty of Economics and Technology, University of the Peloponnese, Akadimaikou G. K. Vlachou Street, GR-22131 Tripoli, Greece; nsagias@uop.gr

*   Correspondence: amoshou@noa.gr; Tel.: +30-21-0349-0152

Abstract: In 2014–2018, four strong earthquakes occurred in the Ionian Sea, Greece. After these events, a rich aftershock sequence followed. More analytically, according to the manual solutions of the National Observatory of Athens, the first event occurred on 26 January 2014 in Cephalonia Island with magnitude $M_L = 5.8$, followed by another in the same region on 3 February 2014 with magnitude $M_L = 5.7$. The third event occurred on 17 November 2015, $M_L = 6.0$ in Lefkas Island and the last on 25 October 2018, $M_L = 6.6$ in Zakynthos Island. The first three of these earthquakes caused moderate structural damages, mainly in houses and produced particular unrest to the local population. This work determines a seismic moment tensor for both large and intermediate magnitude earthquakes ($M > 4.0$). Geodetic data from permanent GPS stations were analyzed to investigate the displacement due to the earthquakes.

Keywords: earthquake; source observations; seismological data; moment tensor inversion; seismicity; Ionian Sea; GNSS; geodetic data

1. Introduction

A detailed analysis of both seismological and geodetic data of the Ionian Islands is performed in this study. It is the first time that such an extensive time period analysis with the latest state-of-the-art software and usage of updated data like the ITRF 2014 reference frame has been applied to Greece's most seismogenic area.

This area is characterized by continuous seismic activity and frequent occurrence of large earthquakes ($M > 6.0$). The tectonic structure of the islands of Cephalonia and Ithaca results from the effect of compressive stresses in which periods of tensile stresses are inserted [1].

The faults kinematics of Cephalonia are classified into the three following categories [2]:

- Reverse faults in the area of Argostoli.
- Strike-slip faults—Argostoli, Paliki and SE Cephalonia area.

The most characteristic tectonic structure is the clockwise fault of Cephalonia (Cephalonia Transform Fault Zone), which consists of Lefkas to the north with a direction of north-west and the part of Cephalonia to the south with the direction north-west [3]. The existence of this transformation fault had been suggested by both studies [4–6] and geological mapping [7–9].

The first seismological indications for horizontal sliding movements in the study area were developed in the 1980s based on epicenters [10] and focal mechanisms of strong earthquakes and aftershocks of 17/01/1983 M = 7.0 and 23/03/1983 M = 6.2, [11,12]. Further study by many scientists confirmed the effect of the horizontal slip fault in the area using synthetic waveform modeling [13], with micro-seismic studies [14] and geodetic measurements [15,16]. The results from the micro-seismic [14,17] and geodetic measurements [15,16] led to the conclusion that this regime extends to the north in the area of Lefkas. Recent studies based on precise epicenters and focal mechanisms confirm the existence of this seismically active fault of Cephalonia that runs parallel to the west coast of Lefkas [3].

The complex seismotectonic structure that controls the wider area's seismicity is the Greek arc section's subsidence zone in the Ionian Sea area below Cephalonia [18].

Figure 1 represents a general structure map showing the prefectures of the broader region of Western Greece. For the study area (Ionian Islands), the portable seismological station sites' selection criterion was based on the existence and operation of permanent seismological and geodetic stations that had already been installed. Faults were collected from the international literature and digitized by ArcGIS Pro.

Aftershock sequences' statistical processing is an essential tool for understanding the earthquake process's focal mechanisms. Changes in the rate of seismicity during seismic sequences indicate precursors to the generation of a strong earthquake during the sequence [19–22]. Detailed seismological data of these large events and the strongest aftershocks were used in this work: The first and significant part focuses on the main event's extensional focal mechanisms and the comparison with those calculated from other institutions. In the second part, using GPS data and calculations of the GPS time series, the coseismic deformation is estimated. The above combination produces precise conclusions about unique seismic sequence characteristics.
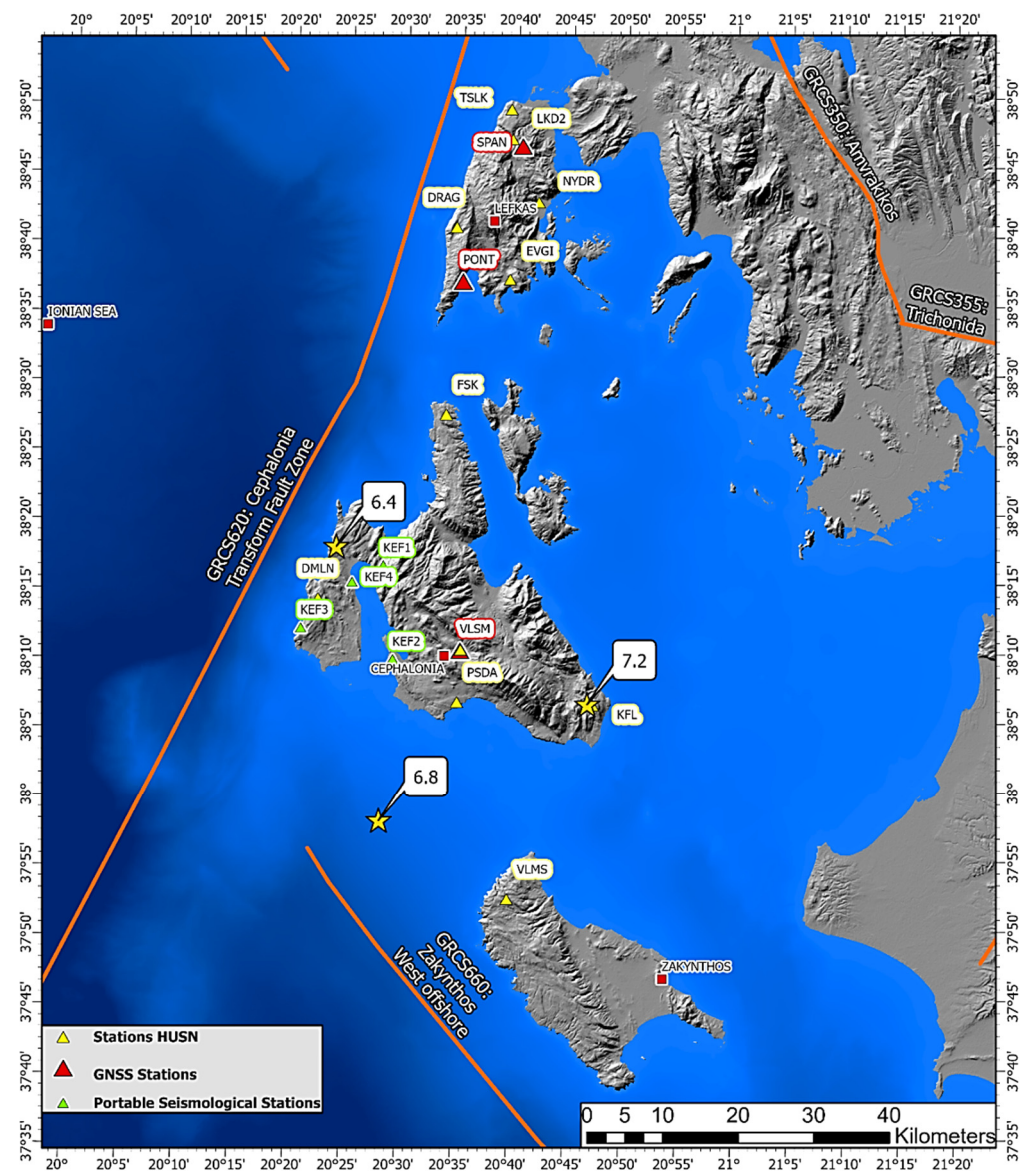
Figure 1. General structure map of the Ionian Sea and the broader area of West Greece; red squares represent the prefectures, while orange lines the main active faults for the study area [23]. Bathymetry is from Emodnet Bathymetr, [23] and DEM. Copernicus Land Monitoring Service, [24] red triangles represent the GNSS network stations, green triangles represent the stations of the portable seismograph network installed immediately after the main earthquake, yellow triangles indicate the permanent stations of the Unified Seismological Network (HUSN), and finally, the three yellow stars indicate the historical earthquake in the region of Cephalonia.

2. Data

In this section, seismological data were used to calculate the seismic parameters of both main earthquakes as well as the major aftershocks of them. The data were collected, analyzed, and processed using an appropriate methodology, analyzed in the next section, and in more detail in [25,26]. GNSS data analysis was performed along with the seismic data to calculate the displacement caused by seismic vibrations and compare it with seismic solutions.

2.1. Seismological Data

In this study, seismological broadband data from the Hellenic Unified Seismological Network were collected and analyzed to determine the source parameters of the events

in the Ionian Sea. For this purpose, 13 broadband stations were equipped with three components seismometers from the Hellenic Unified Seismological Network (HUSN); detailed information is presented in Table 1.

Table 1. Characteristics of Seismological stations in the broader area of Greece. Station coordinates are in decimal degrees; elevation is in m. Sources: [27–30].

Name of the Station	Location	Latitude (°)	Longitude (°)	Elevation (m)	Datalogger	Seismometer
A.G.G.	Agios Georgios	39.02110	22.33600	625	TRIDENT	CMG-3ESP/100
ANKY	Antikythira Island	35.86704	23.30117	143	PS6-SC	Guralp-3ESPC/60
EVR	Karpenisi Evritania	38.91657	21.81050	1037	DR24-SC	Guralp-3ESPC/60
IGT	Igoumenitsa	39.53150	20.32990	262	HRD-24	CMG-3ESP/100
IMMV	Chania Crete	35.46060	23.98110	230	PS6-SC	STS-2
ITM	Ithomi Messinia	37.17872	21.92522	423	DR24-SC	STS-2
JAN	Janena	39.65616	20.84874	526	DR24-SC	Guralp-3ESPC/60
KEK	Kerkira Island	39.71270	19.79623	227	DR24-SC	STS-2
KRND	Kranidi	37.38300	23.15020	140	TAURUS	CMG-3ESP/100
MAKR	Makrakomi	39.01320	22.13170	532	CMG-DM24S6-EAM	CMG-40T
MHLO	Milos Island	36.68984	24.40171	175	PS6-SC	Le3D/20
THL	Klokotos Thessalia	39.56468	22.01440	86	DR24-SC	STS-2
PYL	Pylos	36.89550	21.74200	220	CMG-3T	Reftek-130

2.2. Geodetic Data

The GPS data (30-s sampling interval) were collected and processed from stations VLSM (Valsamata Cephalonia), SPAN (Spanohori Lefkas), PONT (Ponti Lefkas) shown in Figure 1, which belong to the national geodetic network of the Institute of Geodynamics —National Observatory of Athens (NOANET; [31]). The exact location and instrument information of the permanent stations are shown in Table 2.

Table 2. Characteristics of GNSS stations in Ionian. Station coordinates are in decimal degrees; height is in m.

Name	Location	LAT	LON	Height	Antenna	Receiver	Data Start	Data End
VLSM	Valsamata (Cephalonia)	38.176	20.588	437.19	LEIAS 10, NONE	LEICA GR10	01 January 2014	30 December 2019
PONT	Ponti (Lefkas)	38.619	20.585	48.81	LEIAX1202, GG NONE	LEICA GRX 1200PRO	01 January 2014	30 December 2019
SPAN	Spanochori (Lefkas)	38.781	20.673	451.34	LEIAX1202, GG NONE	LEICA GRX 1200PRO	01 January 2014	30 December 2019

After collecting GPS raw data from the online repository, a preprocessing procedure was applied to assure the best quality of post-processing results. TEQC software [32] was used to identify data incompatibilities, excess multipath, and data gaps.

3. Methods

3.1. Fault Plane Solutions

In this section, the Moment Tensor Solution for the strong events and all the moderate earthquakes from each aftershock sequence were calculated and presented. For this purpose, seismological broadband data from the Hellenic Unified Seismological Network (HUSN) were collected, analyzed, and used to determine the fault plane solution, the Moment Magnitude (M_w), and the Depth (d) of the strongest earthquakes of the K1,2, L1 and Z1 sequence.

A methodology based on a moment tensor inversion was used, as analytically described in [26,33,34] using Ammon's software [35]. This method calculates synthetic seismograms directly compared with the observed ones for a given velocity structure. As implemented by Randall [36], Kennett's reflectivity method was applied to determine the Green Functions. Synthetics for the three fundamental faults are combined with an appropriate 1-D velocity model, which, in our case, is the one proposed by Haslinger [37]. The Haslinger velocity model was used. Initially, Green's functions for different depths

were calculated. Regional data of five 3-component broadband stations belonging to the HUSN and situated at different azimuth coverage and epicentral distances less than 3° were selected and analyzed.

Initially, Green's functions for different depths were calculated by the analyst. Initial inversions were performed at a depth interval of 5 km followed by a finer one every 1–2 km around the depth that exhibited the lowest misfit.

Regional data of five broadband stations, at different azimuth coverage and epicentral distances less than 3°, equipped with three components seismometers, were selected and analyzed. The first step of the procedure is preparing the data, including the deconvolution of instrument response, the integration of the velocity to displacement, and the horizontal components' rotation to radial and transverse. Then the long period part of the signal was introduced to perform the inversion. After several attempts, our analysis was implemented using a seismic wave velocity model considered the most appropriate area under study. A bandpass filter is applied to both the observed waveforms and synthetics. We used a frequency band between 0.05 and 0.02 Hz, although the moderate magnitudes were in the range of $4.0 \leq M_w \leq 4.5$. In all our inversions, we use a fixed waveform length of 80 s (the inversion results indicate that inverting waveforms longer than 80 s resulted in higher misfits). Moment tensor solutions' quality can be evaluated by considering the average misfit and the compensated linear vector dipole (CLVD; Column 9, Tables A1–A3). There is a quality code that consists of the letters A–D for each solution for the minimum misfit and between the numbers 1–4 (Quality; Column 11, Tables A1–A3) for the percent of CLVD [38,39].

a   Cephalonia Seismic Sequence

The area of Cephalonia is characterized by too high seismicity, as shown by the past, for example, the seismic action of August 1953 with earthquakes of magnitude 6.5, 6.8, and 7.2 leveled Kefalonia, Zakynthos, and Ithaca and caused about 480 human casualties. The geodynamics and seismotectonic of the area are particularly complex [3,18]. After the destructive sequence of 1953, the strongest earthquakes that have taken place on the broader area are the one west of Cephalonia on 17 January 1983 with $M_L = 7.0$, [10,13] and the one on 18 January 1997 with $M_L = 6.6$ in the Strofades islands. The recent earthquake filled a seismic gap in the area.

On 26 January 2014 (13:55, UTC), two strong earthquakes of magnitude $M_w = 6.1$ and $M_w = 5.2$ (18:45, UTC) occurred in the island of Cephalonia, central Ionia Sea. These events induced extensive structural damages, mainly in the western and central parts. Eight days later, on 3 February 2014 (03:08, UTC), a second strong event with a magnitude similar to the first ($M_w = 6.0$) happened at the north section of Lixouri town. The geographical coordinates for the first events were manually located for this study and found $\varphi = 38.252°$ N, $\lambda = 20.443°$ E at a depth of 16 km. These two earthquakes ($M_w = 6.1$ and $M_w = 6.0$) occurred in the Cephalonia island as the destructive events of 1953. In the first days of August 1953 (9 August 1953 and 12 August 1953), three earthquakes of magnitude 6.4, 6.8, and 7.2 [2] took place in Cephalonia. For these three strong events, the source parameters were calculated and compared to the observed solutions from other institutes, and for the majority of them, a good agreement was found (Table 3). A large number of aftershocks followed these events. We note that 2462 events were recorded and analyzed for the first month, while from the beginning of the sequence until the end of 2019 more than 17,000 events took place and were recorded and viewed as a point cloud [40–42]. In Figure 2, the 3-D view clearly defines the earthquake epicenters depth zones that may overlay in a 2-D representation. From this catalog and for the largest events ($M_w > 3.8$), the activation fault, the Source Parameters, the Seismic Moment (M_0) and the Moment Magnitude (M_w) were calculated using the moment tensor inversion [26].
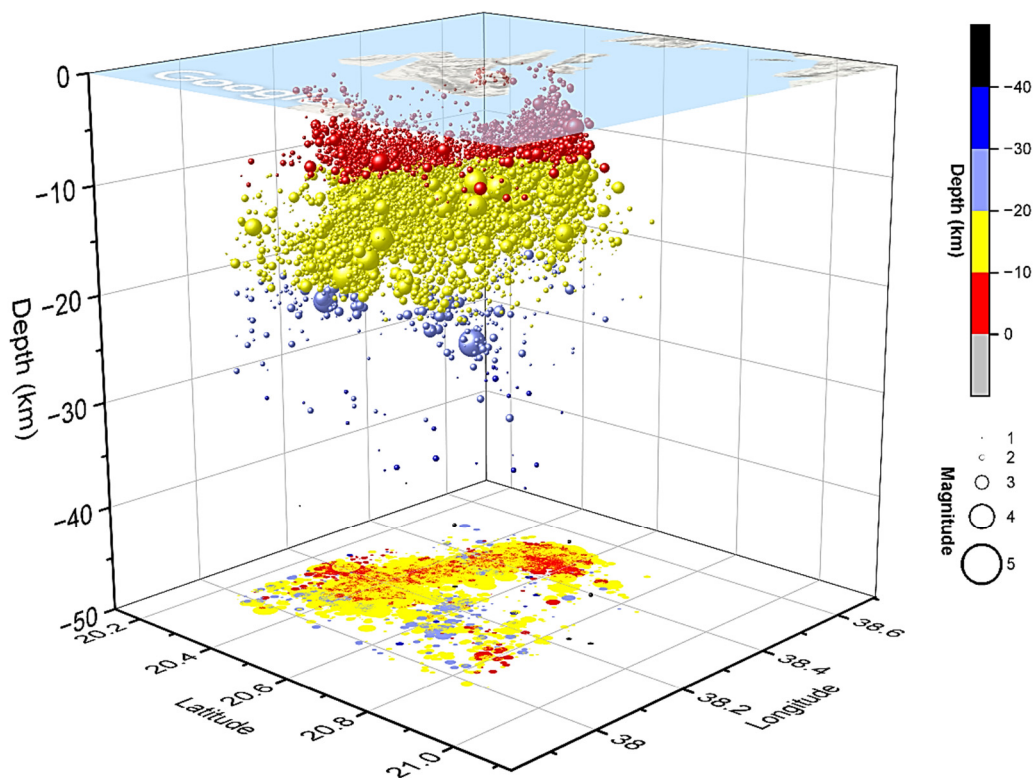
Figure 2. 3-D distribution of epicenters relative to the seismic sequence's depth and magnitude in Cephalonia Island for 2014–2019.

Immediately after the earthquake on 26 January 2014, in Paliki of Cephalonia, the Geodynamic Institute sent a team of scientists and technicians. They installed a portable network of four stations (KEF1, KEF2, KEF3, and KEF4) since the number of existing permanent stations was insufficient for detailed recording of aftershock-seismic activity [43,44]. The significant result of the portable network installation was the possibility of recording thousands of earthquakes (*n* > 8000) over a year, with magnitudes M > 1.0, as seen in Figure 3. The seismological portable network's geographical distribution and the data used from the permanent seismological network stations for the inversion appear in Figure 1.

Using the methodology described in the previous Section 3.1 and in the study [26] the Source Parameters (φ, δ, λ), the Moment Magnitude (M_w), the Seismic Moment (M_0) and the depth were calculated and are presented in Figures 4–6 regarding the three strongest earthquakes in Cephalonia Island.

The Scheme 26 January 2014 (18:45 UTC), a few hours later, a second of magnitude Mw = 5.2 occurred in the same region as the first event. Using waveforms from Unified Seismological Network (HUSN), the epicenter was manually located at 38.1423° N, 20.2812° E. Broadband recordings from the HUSN network were collected, and those at epicentral distances less than 3° degrees were selected. For the inversion method, five stations were used with good azimuthal coverage. Reverse type faulting was revealed after applying the previous methodology. The obtained focal mechanism is φ = 19°, δ = 62° and λ = 170°. The seismic moment is equal to Mo = 5.99 × 10^{23} dyn·cm, for a focal depth equal to 20 km. The inversion resulted in a double couple (DC) equal to 91%, while the compensated linear vector dipole was equal to 9% (Figure 5).

Next, we present the results of inversion for the third-largest earthquake of this seismic sequence. This earthquake showed specificity as to the application of the method mainly because of its geographical position. The epicenter was calculated in the NW part of Cephalonia Island, according to the National Observatory of Athens (φ = 38.2462° N, λ = 20.3958° E). Due to insufficient azimuthal coverage of the Greek stations, trials were made for some fault plane solutions being recalculated by adding records either of Italian

stations, either in mixed epicentral distances, more than 300 km, thus extending our azimuthal coverage to the west and south of the epicenter. To compute the focal mechanism of six stations for three components, each one was used in epicentral distances between 130 and 380 km to determine this event's source parameters. The source parameters were calculated using the method of moment tensor inversion outlined previously. The best fit solution is: strike = 20°, strike = 67°, rake = 174°, and the focal depth was calculated at 20 km. The seismic moment is determined as $M_o = 2.46 \times 10^{24}$ dyn·cm, and the calculated double couple (DC) was found equal to 88%, while the compensated linear vector dipole (CLVD) to 12%. The results of the applied procedure are presented in Figure 5.
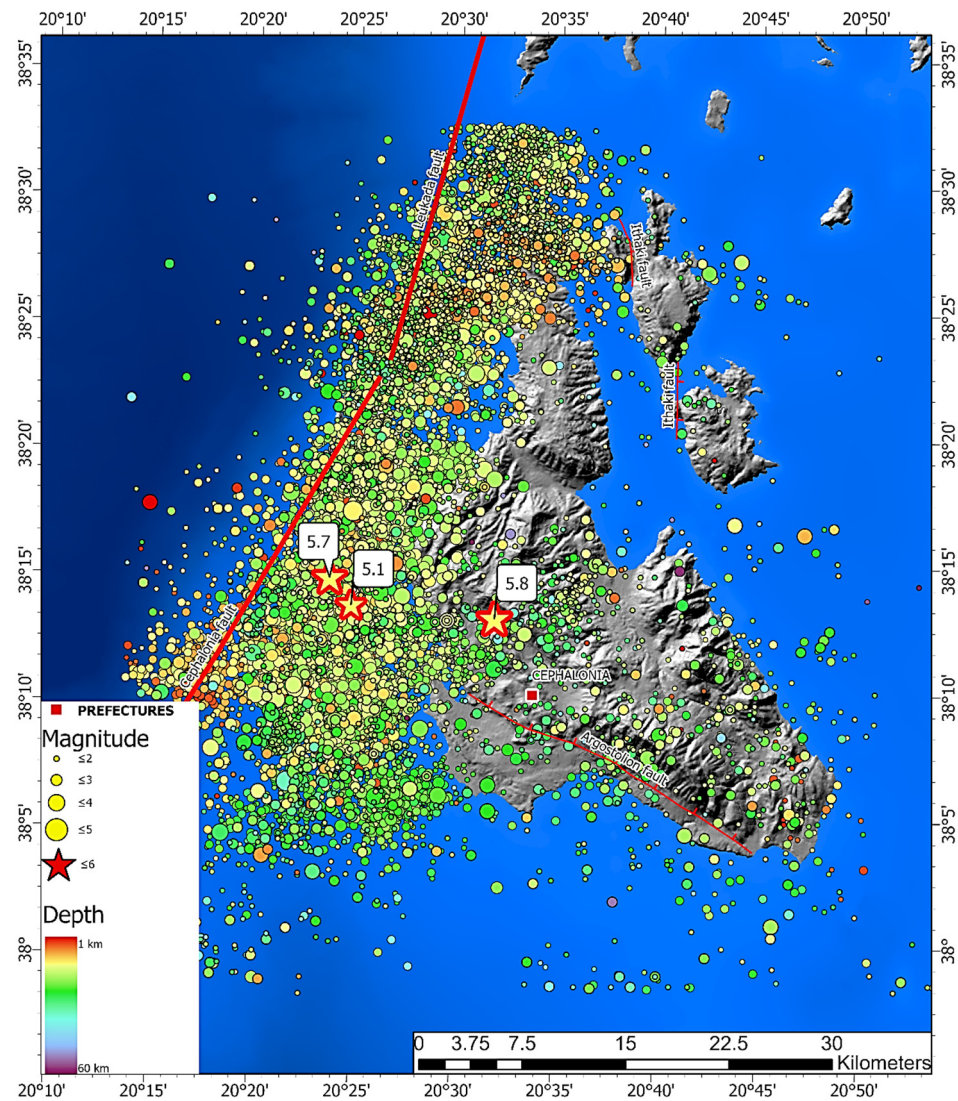
Figure 3. The 26 January 2014 (M_L = 5.8, 5.1—yellow stars), 3 February (ML = 5.7—yellow star), and aftershock epicenters were recorded and manually calculated by the scientific team of the peaking of National Observatory of Athens (NOA—[27]) until 31 December 2019. Distribution of the epicenters for the time period 2014–2019 size and color of the points according to magnitude and depth.
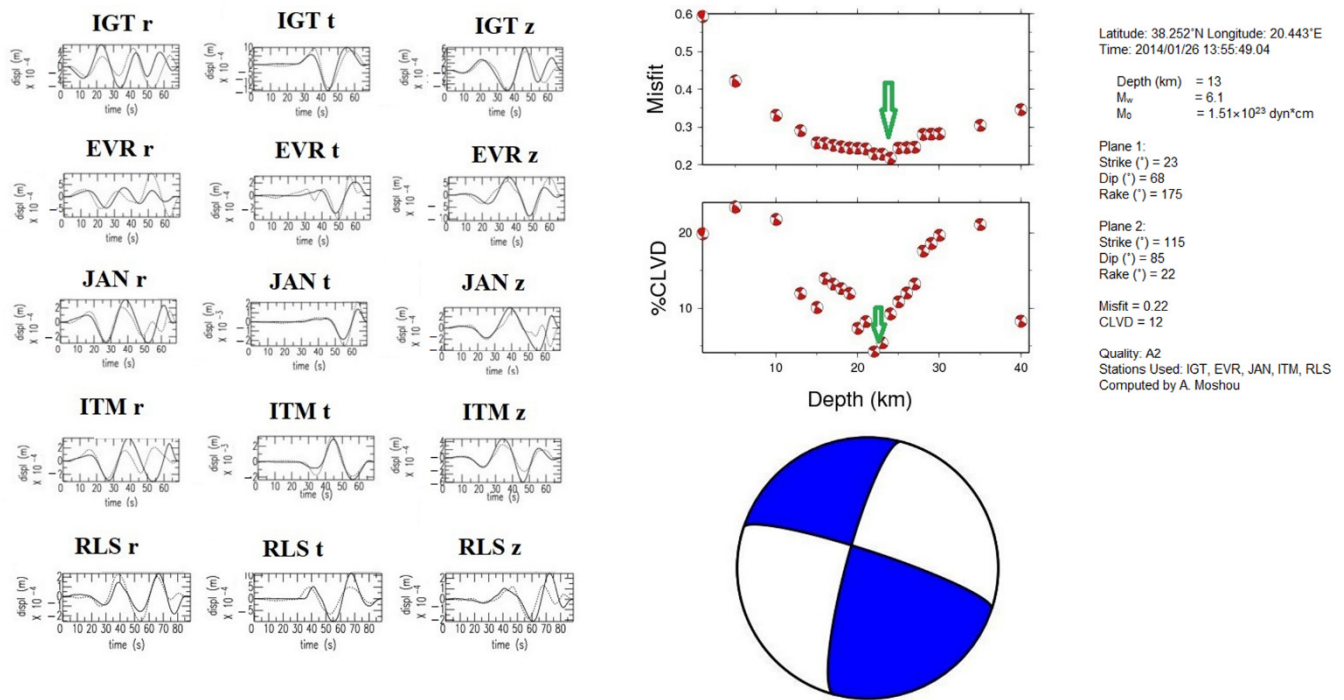
Figure 4. Moment tensor solution of the 26 January 2014 (13:55 UTC) earthquake. The selected solution is highlighted with the green arrow in the misfit/compensated linear vector dipole (CLVD)-versus-depth diagrams (center-up). The summary of the solution and the corresponding beach ball is shown in the center-low. The observed and synthetic displacement waveforms (continuous and dotted lines, respectively) are shown at the left, at the inverted stations for the radial, tangential and vertical components. At left-center-right and up-middle-low, the summary of the solution and the fault plane solution as lower hemisphere equal-area projection are depicted.
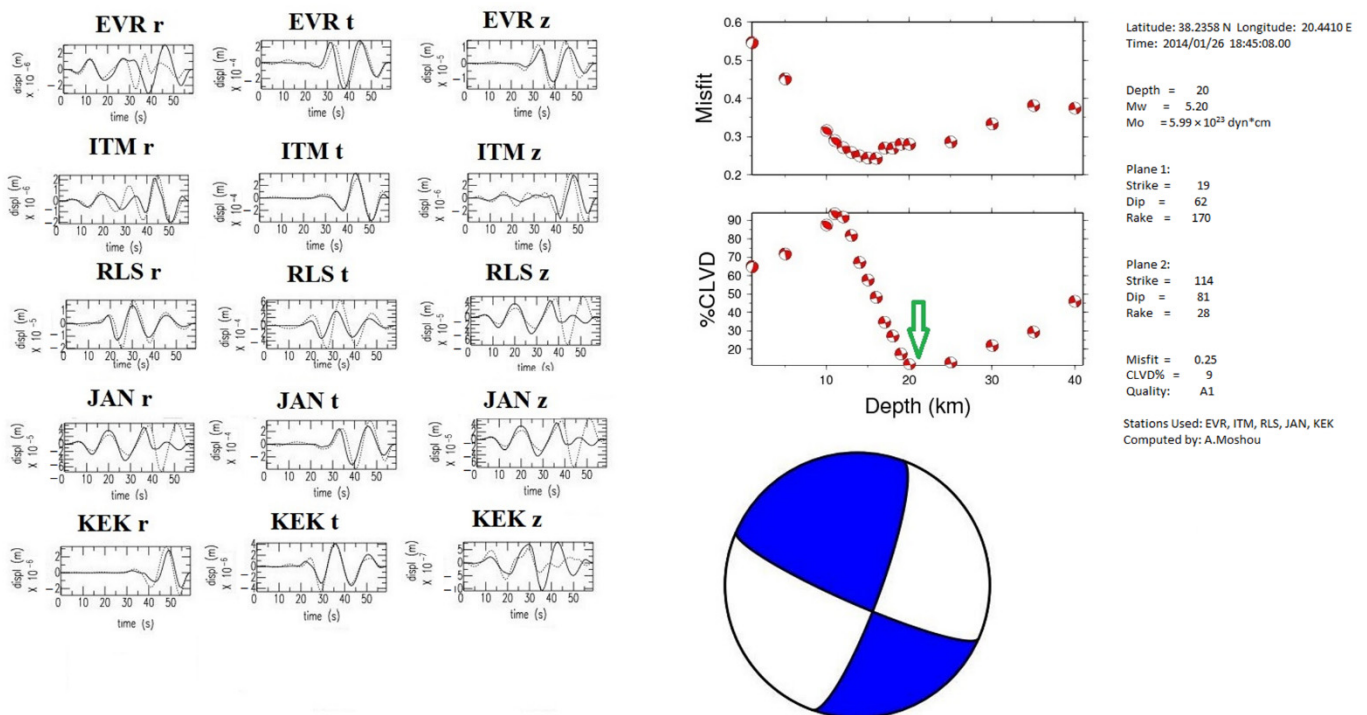
Figure 5. Moment tensor solution of the 26 January 2014 (18:45 UTC) earthquake. The selected solution is highlighted with the green arrow in the misfit/compensated linear vector dipole (CLVD)-versus-depth diagrams (center-up). The summary of the solution and the corresponding beach ball is shown in the center-low. The observed and synthetic displacement waveforms (continuous and dotted lines, respectively) are shown at the left, at the inverted stations for the radial, tangential

and vertical components. At left-center-right and up-middle-low, the summary of the solution and the fault plane solution as lower hemisphere equal-area projection are depicted.

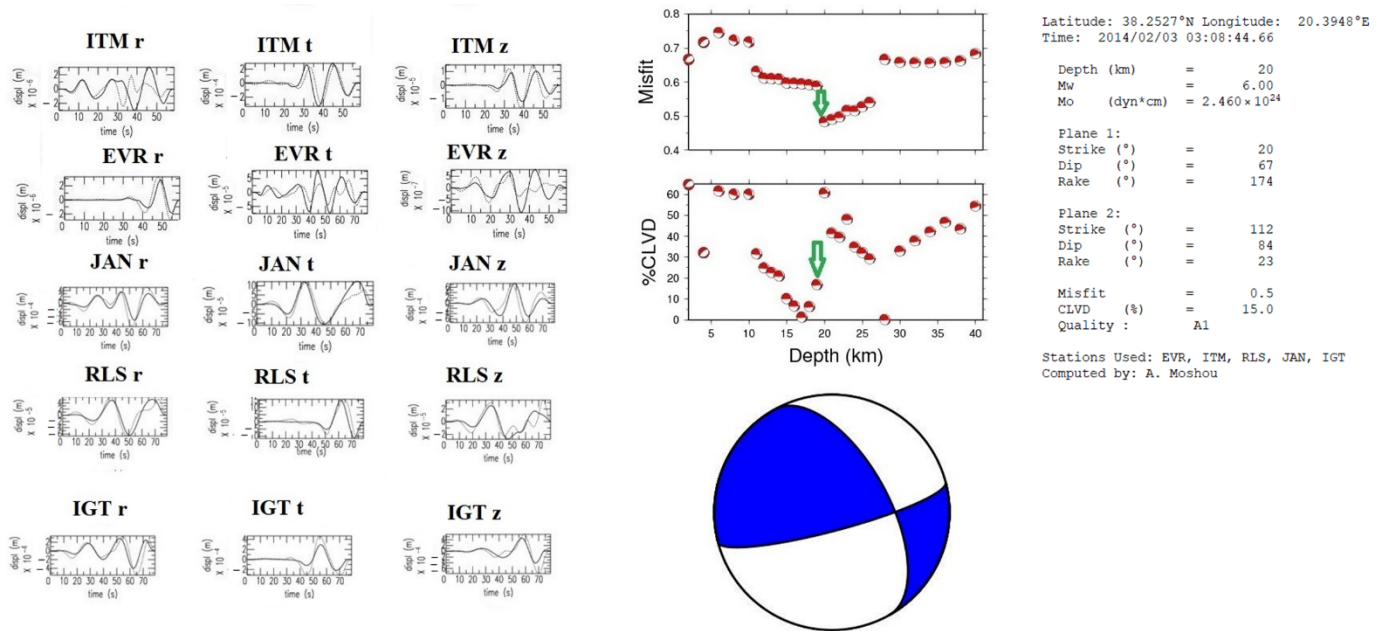**Figure 6.** Moment tensor solution of the 3 February 2014 (03:08 UTC) earthquake. The selected solution is highlighted with the green arrow in the misfit/CLVD-versus-depth diagrams. Below this appears the summary of the solution and the corresponding beach ball. The left of the figure shows the misfit/CLVD diagrams observed and synthetic displacement waveforms (continuous and dotted lines, respectively) at the inverted stations for the radial, tangential and vertical components. In the lower part of the figure, the solution's summary and the fault plane solution as lower hemisphere equal-area projection are depicted.

Table 3. List of Moment Tensor Solutions published by various Institutions for Cephalonia earthquakes' main shocks (January–February 2014). Source: [45].

Institute	Lat (°)	Lon (°)	M_w	M_0 (dyn*cm)	Depth (km)	Strike (°)	Dip (°)	Rake (°)	Strike (°)	Dip (°)	Rake (°)
Cephalonia Earthquake (26 January 2014, 13:55:43.04, UTC) Mw = 6.1											
Our Study	**38.252**	**20.443**	**6.1**	**1.510×10^{23}**	**13**	**23**	**68**	**175**	**115**	**85**	**22**
NOA	38.220	20.390	6.0	1.250×10^{28}	6	18	67	164	114	75	24
HARV	38.150	20.360	6.1	2.040×10^{25}	14	20	65	177	111	87	25
INGV	38.170	20.370	6.1	1.700×10^{25}	10	290	81	−1	20	89	−171
KOERI	38.283	20.598	5.8	9.570×10^{24}	16	16	87	−174	286	84	−3
GFZ	38.250	20.450	6.1	2.000×10^{25}	17	289	85	4	198	86	175
CPP	38.200	20.400	6.2	2.120×10^{25}	19	10	49	159	114	74	42
GEOAZUR	38.208	20.425	6.2	2.120×10^{25}	6	15	68	165	111	76	22
AUTH	38.260	20.590	6.1	1.360×10^{28}	10	286	90	−5	16	85	−180
UOA	38.213	20.467	6.1	2.030×10^{25}	16	30	70	169	124	80	20
Cephalonia Earthquake (26 January 2014, 18:45:08.02, UTC) Mw = 5.3											
Our Study	**38.235**	**20.441**	**5.2**	**5.990×10^{23}**	**20**	**19**	**62**	**170**	**114**	**81**	**28**
NOA	38.236	20.442	5.3	1.030×10^{27}	6	149	64	65	16	35	131
HARV	38.100	20.250	5.5	2.020×10^{24}	17	16	39	138	141	65	59
INGV	38.120	20.280	5.5	2.200×10^{24}	17	15	38	139	140	66	60
GFZ	38.290	20.340	5.4	1.400×10^{24}	15	173	50	91	352	40	89
AUTH	38.230	20.370	5.3	1.410×10^{24}	9	20	39	123	160	58	66
Cephalonia Earthquake (03/02/2014, 03:08:44.66, UTC) Mw = 6.0											
Our Study	**38.246**	**20.396**	**6.1**	**1.630×10^{25}**	**12**	**176**	**58**	**145**	**286**	**61**	**37**
NOA	38.253	20.395	5.9	1.020×10^{28}	3	13	75	163	108	73	15
HARV	38.120	20.370	6.0	1.490×10^{25}	12	12	45	154	120	72	48
USGS	38.190	20.340	6.0	1.490×10^{25}	16	356	50	127	126	52	54
INGV	38.200	20.390	6.1	2.000×10^{25}	8	13	43	161	118	77	49
KOERI	38.260	20.320	5.8	9.570×10^{24}	60	317	66	59	193	38	139

Table 3. *Cont.*

GFZ	38.230	20.390	6.0	1.300×10^{25}	14	183	56	138	300	56	43
CPP	38.300	20.300	6.4	4.270×10^{25}	15	142	82	84	355	10	122
AUTH	38.270	20.320	6.0	9.640×10^{24}	7	287	87	−3	17	87	−177
UOA	38.269	20.388	5.9	9.600×10^{24}	5	35	62	175	127	86	28

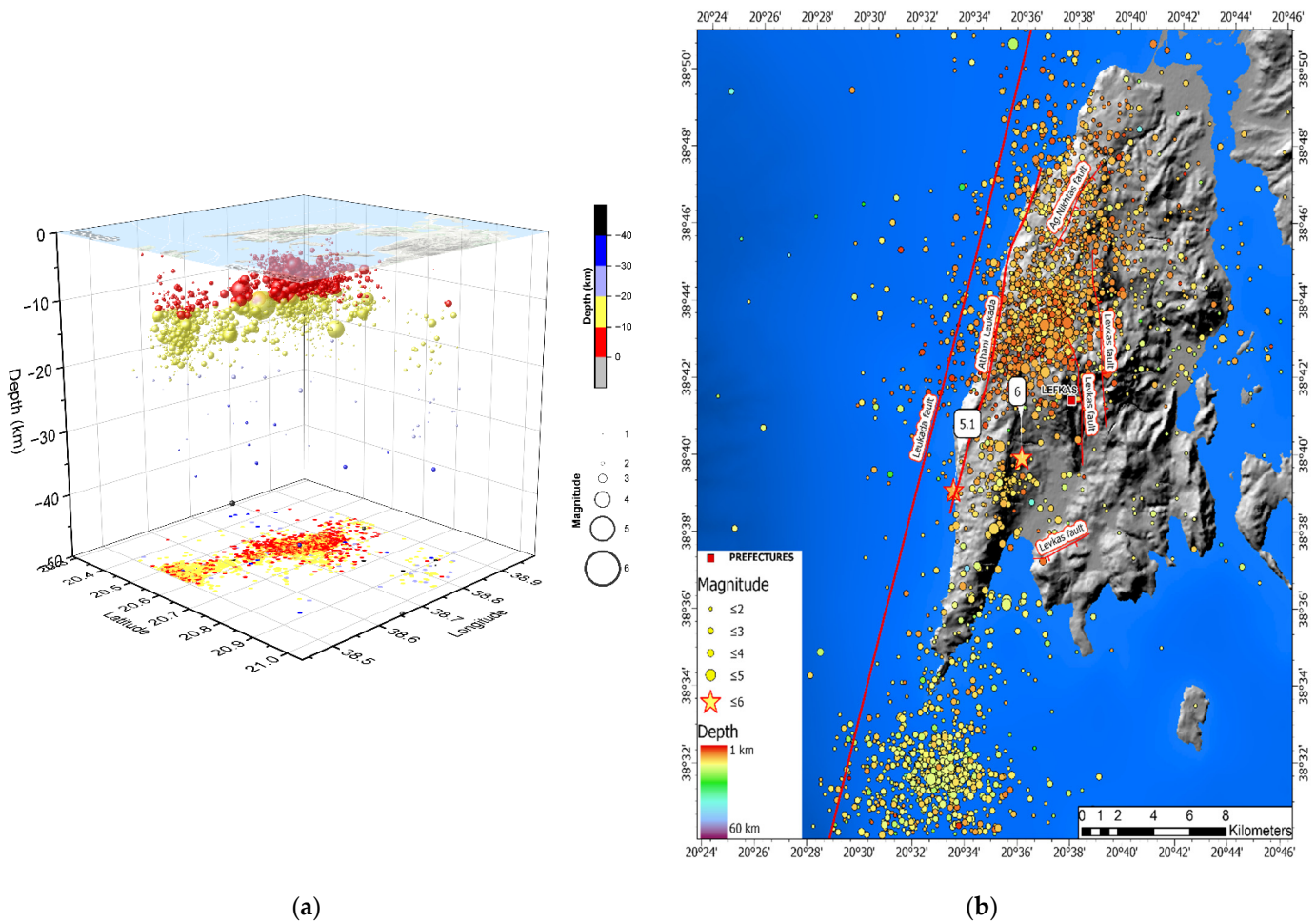b   Lefkas Seismic Sequence

A strong earthquake with a magnitude $M_w = 6.4$ occurred in Lefkas Island, Greece. The geographical coordinates, as they calculated from the manual analysis of the Institute of Geodynamics—NOA [27] are $\varphi = 38.6655°$ N, $\lambda = 20.6002°$ E at a depth of 10 km. A few hours later, a second strong event with magnitude $M_L = 5.0$ occurred in the same region. These earthquakes caused much structural damage to Agios Petros, Athani, Dragano, and Komilio [46,47] and environmental effects, including liquefaction, extensive rockfalls, and landslides, [48]. No surface ruptures were found in the field. The most recent strong earthquake occurred on 14 August 2003 with a magnitude of $M_w = 6.2$, offshore the western coast of Lefkas Island, causing severe damages around the whole island [49,50].

A rich seismic sequence followed these events for the following days. More specifically, from 17 November 2015 until the end of the month, 837 events were recorded, while for the first 24 h, the recorded events were 206. The 3D distribution of the epicenters compared to depths and the magnitudes and the distribution of the aftershocks relative to the years is shown in Figure 7a,b.

All the focal mechanisms from events with magnitude $M_w > 4.0$ were calculated using the proposed methodology (Appendix A, Table A2). The source parameter and the focal mechanism for the main event are shown in Figure 8. For this purpose, the data of six stations of three components, each one in epicentral distances less than 350 km, were used. The source parameters were calculated using the method of moment tensor inversion outlined previously. For the main event, the inversion indicates the activation of a strike-slip type faulting. The best fit solution is strike = 290°, strike = 88°, rake = −12°, and the focal depth is calculated at 10 km. The seismic moment was determined as $M_0 = 4.402 \times 10^{28}$ dyn·cm, and the calculated double couple (DC) was found equal to 85%, while the compensated linear vector dipole (CLVD) to 15%. The following table (Table 4) presents the moment tensor solutions from various institutions for the 17 November 2015 Lefkas earthquake.

Table 4. List of Moment Tensor Solutions published by various Institutions for the 17 November 2015 earthquake (07:10, UTC) Source: CSEM—EMSC, [45].

Lefkas Earthquake (17 November 2015, 07:10:07.30, UTC) $M_w = 6.4$											
Institute	Lat (°)	Lon (°)	M_w	M_0 (dyn*cm)	Depth (km)	Strike (°)	Dip (°)	Rake (°)	Strike (°)	Dip (°)	Rake (°)
Our Study	**38.6655**	**20.6002**	**6.4**	**4.400×10^{25}**	**10**	**290**	**88**	**−12**	**20**	**82**	**−178**
NOA	38.6662	20.5957	6.4	4.400×10^{25}	10	203	88	159	293	69	2
USGS	38.7659	20.5576	6.5	6.690×10^{25}	15	293	86	−9	23	80	−176
GFZ	38.7900	20.4700	6.4	4.600×10^{25}	13	112	87	6	22	84	177
HARVARD	38.5000	20.5100	6.5	6.920×10^{25}	14	24	69	−176	292	87	−21
INGV	38.6200	20.3200	6.5	5.700×10^{25}	13	23	71	179	113	89	19
IPGP	38.7550	20.5520	6.6	9.980×10^{25}	13	295	85	−18	27	72	−175
CPPT	38.7800	20.6300	6.5	6.170×10^{25}	15	294	80	−5	24	85	−170
AUTH	38.6600	20.6000	6.3	4.960×10^{25}	12	201	80	142	299	53	13
UPSL	38.6757	20.5720	6.4	5.270×10^{25}	12	211	67	−165	115	77	−24

(**a**)   (**b**)

Figure 7. (**a**) 3-D distribution of epicenters for the seismic sequences in Lefkas Island for the time period 17 November 2015–31 December 2019 with a total number of events *n* = 2804. The red color marks the epicenter with depths under 10 km, the yellow color the epicenter of this sequence with depths between 10 km < d < 20 km, and the blue color the epicenters with depths between them 30 km < d < 40 km. All the epicenters' depths were taken as calculated from the manual analysis of the National Observatory of Athens, [51], by selecting the study area and the time interval; (**b**) distribution of epicenters for the seismic sequences in Lefkas Island for 17 November 2015–31 December 2019 with a total number of events *n* = 2804. All the epicenters were taken as calculated from the manual analysis of the National Observatory of Athens, [51] by selecting the study area and the time interval. The size and color of the points are dependent on magnitude and depth accordingly.
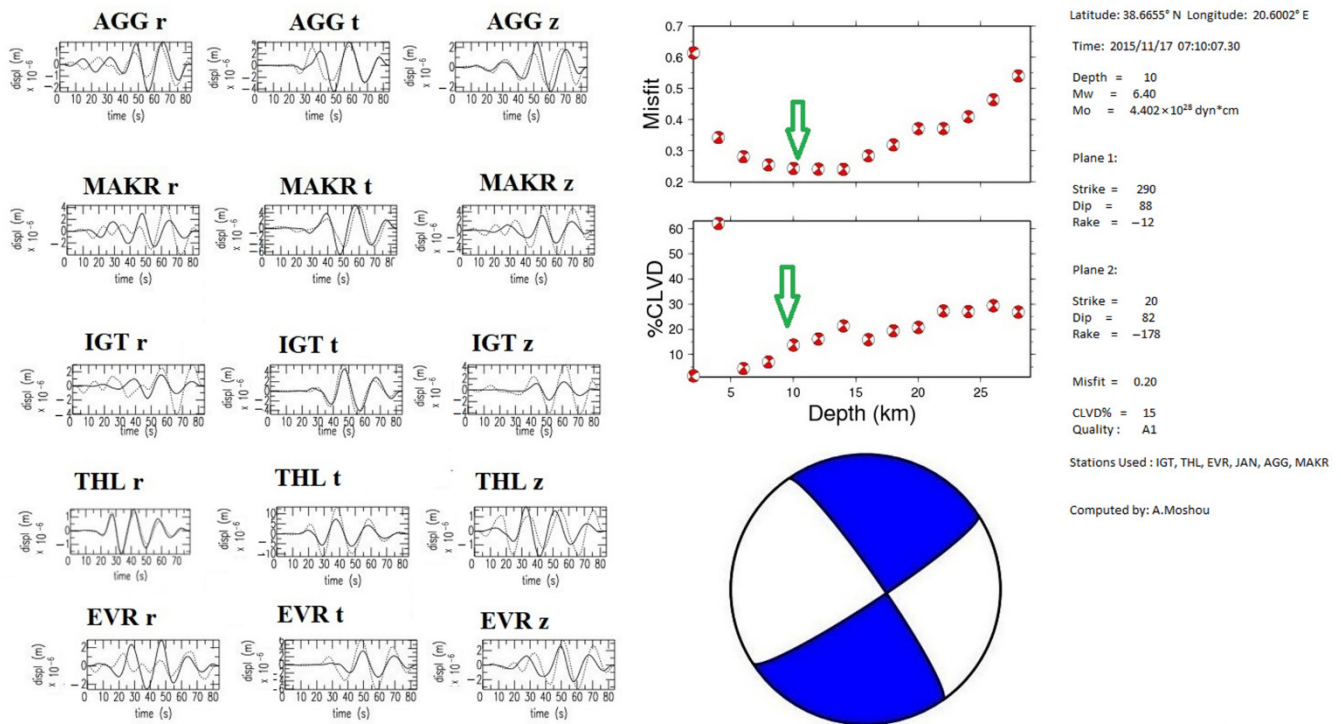
Figure 8. Moment tensor solution of the 17 November 2015 (07:10 UTC) earthquake. The selected solution is highlighted with the green arrow in the misfit/CLVD-versus-depth diagrams (center-up). The summary of the solution and the corresponding beach ball is shown in the center-low. The observed and synthetic displacement waveforms (continuous and dotted lines, respectively) are shown at the left, at the inverted stations for the radial, tangential and vertical components. At left-center-right and up-middle-low, the summary of the solution and the fault plane solution as lower hemisphere equal-area projection are depicted.
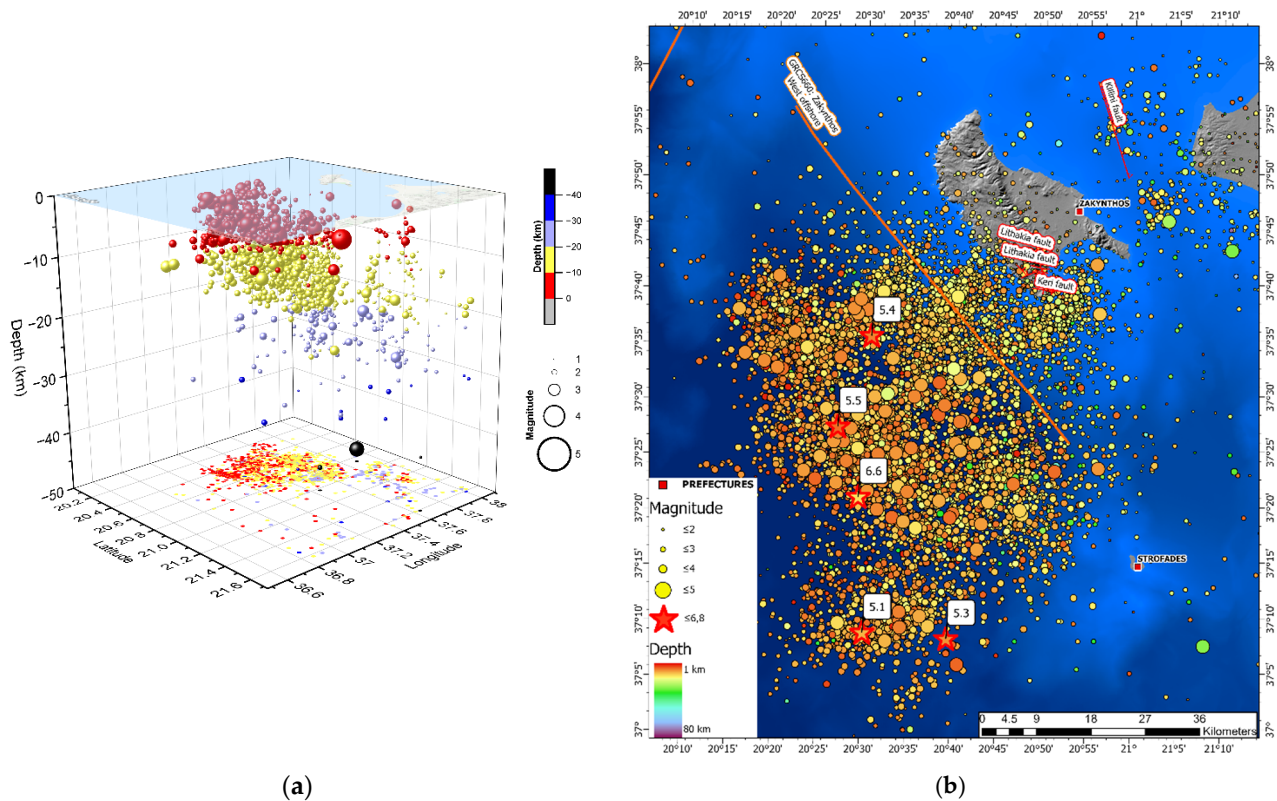
c   Zakynthos Seismic Sequence

On 25 October 2018 (22:54 UTC) a strong shallow earthquake with magnitude M_w = 6.7 occurred offshore Zakynthos (Ionian Sea, Greece). The epicenter calculated was located φ = 37.341° N, λ = 20.512° E, 40 km southwest of the island of Zakynthos, Ionian Sea, Greece, [52–54].

A large number of aftershocks that followed this event appears in Figure 9a,b. The most recent seismic sequence occurred during April–May 2006. It consists of four moderate earthquakes (5.3 $\leq M_w \leq$ 5.7) that were followed by significant seismic activity. Those focal mechanisms were calculated in the study [55].

All the focal mechanisms from events with magnitude M_w > 4.5 were calculated (Appendix A, Table A3). To determine the source parameters, the data of five stations of three components, each one in epicentral distances less than 350 km, were used. The source parameters were calculated using the method of moment tensor inversion outlined previously. Thrust type faulting was revealed after applying moment tensor inversion. The best fit solution was strike = 123°, strike = 42°, rake = 30°, and the focal depth was calculated at 17 km. The seismic moment was determined at M_0 = 1.45 × 10^{26} dyn·cm, and the calculated double couple (DC) was found equal to 80%, while the compensated linear vector dipole (CLVD) to 20%. The result of the applied modeling is presented in Figure 10. The following table (Table 5) presents the moment tensor solutions from various institutions for the 25 October 2018 Zakynthos earthquake.

Table 5. List of Moment Tensor Solutions published by various Institutions for the 25 October 2018 earthquake (22:54, UTC). Source: CSEM—EMSC.

Institute	Lat (°)	Lon (°)	M_w	M_0 (dyn*cm)	Depth (km)	Strike (°)	Dip (°)	Rake (°)	Strike (°)	Dip (°)	Rake (°)
Zakynthos Earthquake (25 October 2018, 22:54:50.00, UTC) M_w = 6.7											
Our Study	**37.3516**	**20.4922**	**6.7**	**1.450×10^{26}**	**17**	**123**	**42**	**30**	**10**	**70**	**128**
NOA	37.3410	20.5123	6.7	1.450×10^{26}	10	108	85	41	14	49	174
USGS	37.5775	20.6859	6.8	1.700×10^{26}	19.5	109	81	51	8	38	166
INGV	37.4900	20.6000	6.8	2.600×10^{26}	25	117	85	63	17	27	168
GFZ	37.5200	20.6600	6.8	2.100×10^{26}	18	107	85	68	5	23	167
GCMT	37.3300	20.6100	6.8	2.310×10^{26}	12	117	84	66	13	24	165
UPSL	37.5300	20.6200	6.8	1.780×10^{26}	10	109	85	42	15	47	173
AUTH	37.3900	20.6300	6.6	8.590×10^{25}	14	273	86	−10	3	80	−179
UOA	37.3601	20.4955	6.6	9.050×10^{25}	20	119	84	66	15	24	164

(**a**)　　　　　　　　　　　　　　　　　　　　　　　　　　　(**b**)

Figure 9. (**a**) Distribution of epicenters for the seismic sequences in Zakynthos Island for the period 25 October 2018–31 December 2019 with a total number of events *n* = 12.629. All the epicenters' depths were taken as calculated from the manual analysis of the National Observatory of Athens dataset [51] selecting the study area and the time interval; (**b**) distribution of epicenters for the seismic sequences in Zakynthos Island for the period 25 October 2018–31 December 2019. All the epicenters were taken as calculated from the manual analysis of the National Observatory of Athens, [51] by selecting the study area and the time interval.
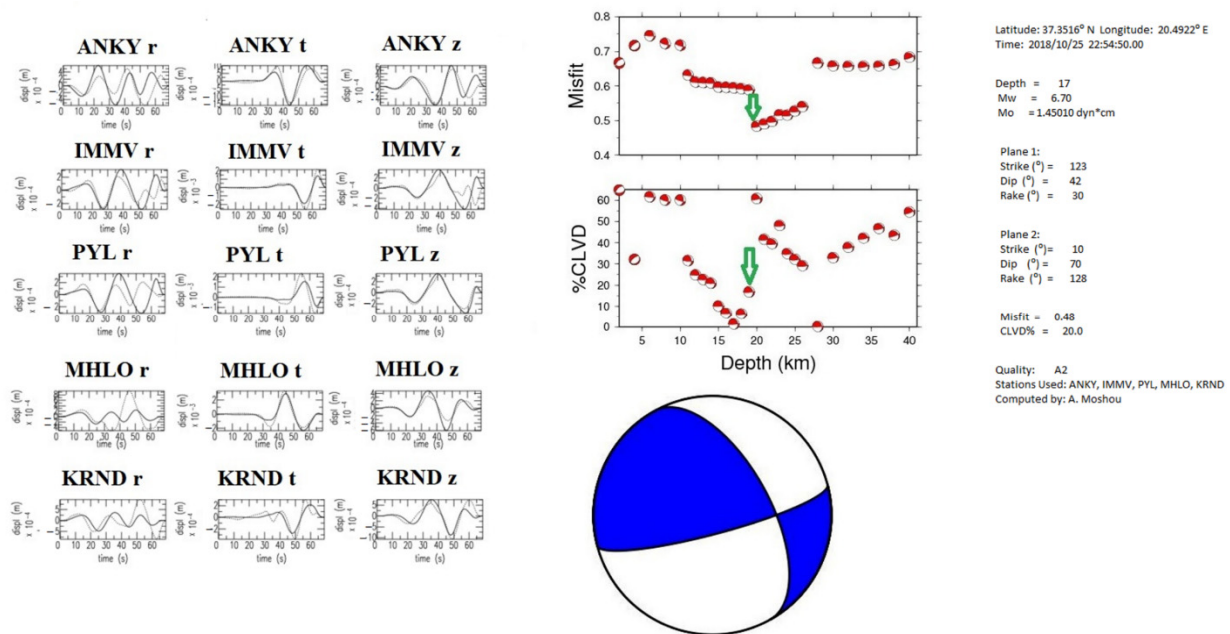
Figure 10. Moment tensor solution of the 25 October 2018 (22:54 UTC) earthquake. The selected solution is highlighted with the green arrow in the misfit/CLVD-versus-depth diagrams (center-up). The summary of the solution and the corresponding beach ball is shown in the center-low. The observed and synthetic displacement waveforms (continuous and dotted lines, respectively) are shown at the left, at the inverted stations for the radial, tangential and vertical components. At left-center-right and up-middle-low, the summary of the solution and the fault plane solution as lower hemisphere equal-area projection are depicted.

3.2. Processing of GPS Data

GIPSY/OASIS II software (ver. 6.4) developed by Jet Propulsion Laboratory (JPL, Pasadena, CA, USA) [56] was used to process our data from GPS. The post-processing software uses the precise Point Positioning strategy (PPP) [57]. This method's main advantage is that only a single specific station is needed to produce results, rather than analyzing tens of stations in a DGPS technique, saving valuable computational resources and time.

The GPS data format was RINEX 2.11 from all the three stations (VLSM, PONT, KLOK), a non-fiducial high precision clock, and orbit files that were used (flinnR_nf from JPL). According to international guidelines and experience [58] (a value of 5×10^8 cm/s^2) random walk noise is recommended; zenith and tropospheric estimation were used. A troposphere mapping function GPT2 (Global Pressure and Temperature Mapping Function) [59] was used, which was shown to be better than the NIELL mapping function [60] and provides similar results as the VMF1 model (Vienna Mapping Function). Because we analyzed long-term recording GNSS stations [61] (we kept the advantage not to maintain a tropospheric database for this purpose), the use of GPT2 was found to be more appropriate. A lower elevation angle cutoff of $10°$ was used to eliminate the near-field multipath effect. Also, a receiver antenna calibration file was calculated and generated for each station separately from the IGS atx file, [62]. WahrK1 [63] tide model was used, and (OcnldCpn) ocean load tide model was added, which uses 11 tidal frequencies to infer other frequencies; After the post-processing procedure, a reference frame transformation to ITRF2014 took place for each station and the time series further analyzed with TSANALYZER [64] to remove any outliers and extract the velocity of each station. The final time series is presented in Figure 11.
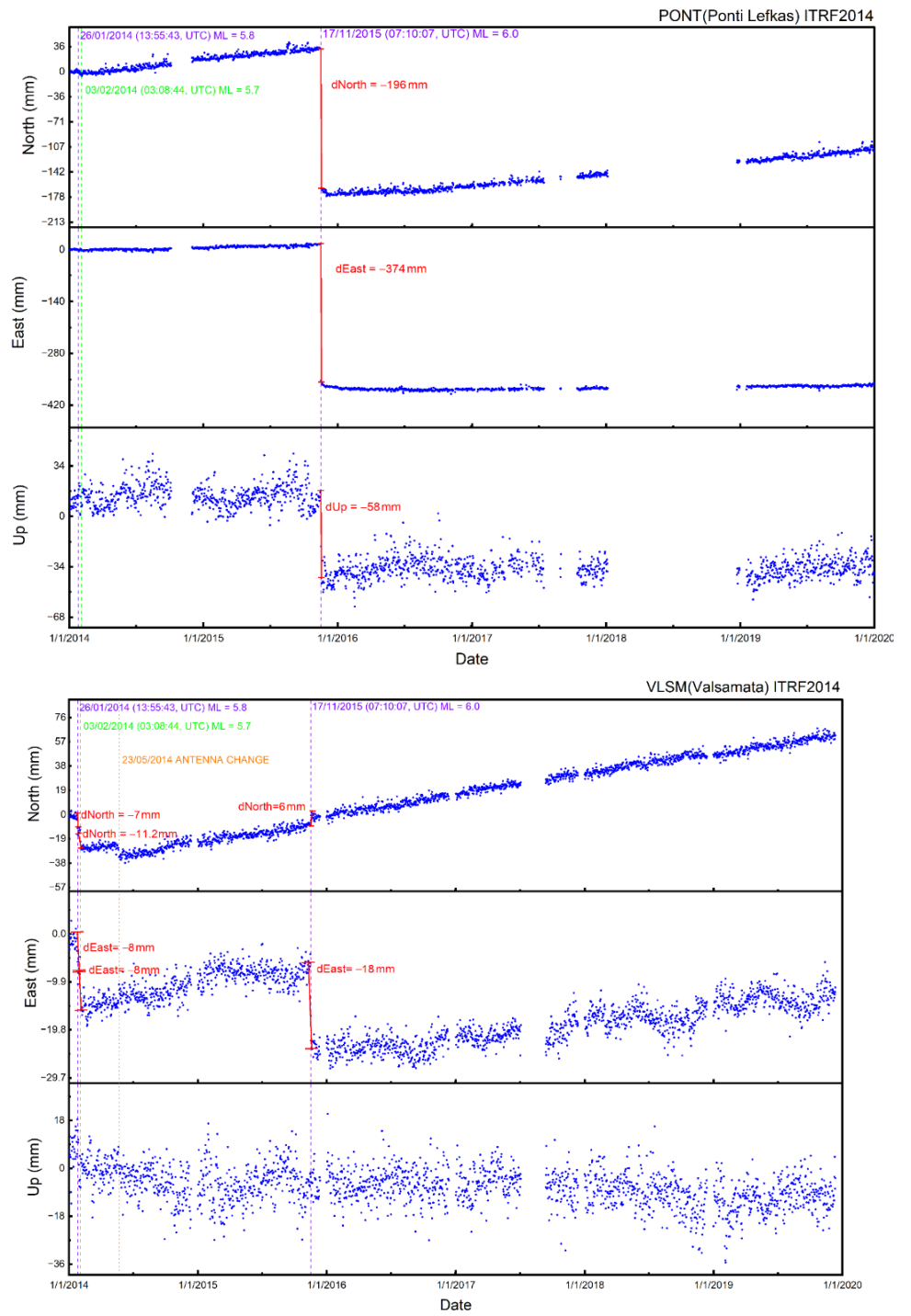
Figure 11. *Cont*.
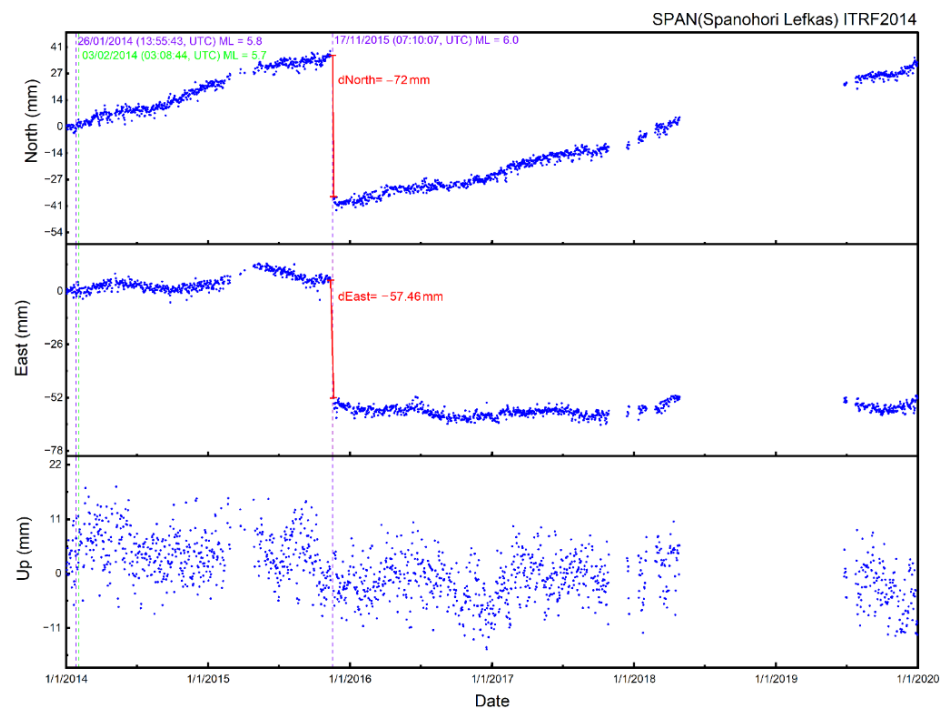
Figure 11. GNSS time series of permanent stations: from the top, Ponti Lefkas (PONT), Valsamata Cephalonia (VLSM) and Spanohori Lefkas (SPAN). Vertical lines show the significant earthquakes in 2014 and 2015 and also shows in 2014 the effect on the time series of the antenna change at station VLSM. The displacement that occurred was marked with a vertical red line. The east displacement scale in Figure 12 was changed (magnified) to better observe the displacement.
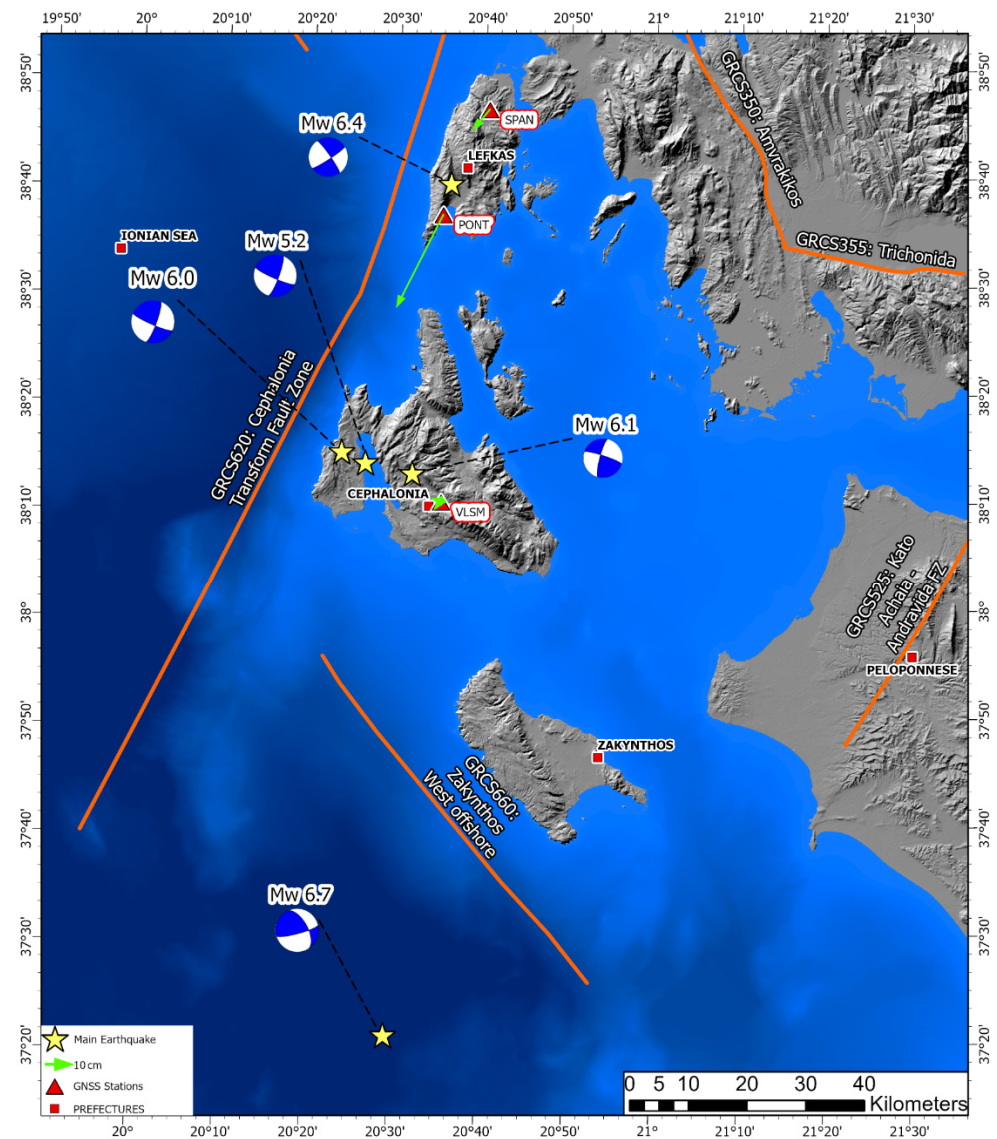
Figure 12. The Ionian region's main earthquakes from 2014 to 2019 with Moment Tensors solutions and major faults from [56], the red triangles represent the permanent GNSS stations with green arrows representing the displacement from Lefkas Earthquake (Mw 6.4) PONT 42.2 cm, SPAN 9.2 cm, VLSM 2 cm.

4. Discussions

Both seismological and geodetic data were used to analyze the strong events during the period 2014–2019 in the Ionian Islands. Source parameters were calculated for the seismic events using regional seismological data. The knowledge of the source parameters for strong as well as for moderate earthquakes is an essential tool for seismically active regions. In general, it allows analytical studies to reveal the tectonics and the seismogenic characteristics of a specific region. The modeling of the strongest earthquakes, using regional data of these sequences, was studied and revealed the region's tectonics, which is characterized by strike-slip and thrust faulting. Strike-slip faulting appears in Cephalonia and Lefkas strong earthquakes, while thrust type faulting appears south of Zakynthos island. Common events were compared with other studies [65,66], and they were found in very good agreement. The main reason to compare this study's solutions with those from other various institutes is to check the proposed methodology's stability as it is applied to earthquakes with different seismotectonic regimes and different magnitude ranges. For

all the events used to calculate the source parameters, the epicenter was recalculated and appears in the first line of Tables 3–5 with bold using the velocity model [37].

To determine fault-plane solutions, a methodology and appropriate software implementing the moment tensor inversion was applied. The method calculates synthetic seismograms directly compared with the observed ones for a given velocity structure. The reflectivity method of Kennett, as implemented by Randall, was applied to determine the Green functions. Synthetics for the three fundamental faults are combined with an appropriate 1-D velocity model, which, in our case, is the one proposed by Hasslinger [37]. The focal mechanisms solutions determined in this study appear in Figure 12.

Moreover, the Geodetic Time Series of all the earthquake sequences was analyzed by PPP methodology, which finds the precise position only using each station and precise orbits and clocks products. The position is independent of long-baseline errors introduced by Differential GPS (DGPS) [67], which may produce over or underestimated displacements. The ITRF2014 reference frame [68] minimizes the error introduced from older reference frames like IGb08 and ITRF2008 seen in other studies [69].

We observe that the Lefkas event caused displacement in a broader area (in stations PONT, SPAN, and VLSM) but the Cephalonia event only in the limited area of Cephalonia (in station VLSM). These data contribute to a clearer understanding that the Lefkas event occurred as a result of the CTF regional system [70,71] in contradiction to the Cephalonia event that occurred as a result of the CTF local faulting system. This evidence is getting stronger by Moment Tensors studies, which are the same at both events.

Future studies should consider that data from more seismological and geodetical stations in the broader area of Ionian will help better understand the local CTF Cephalonia faulting structure; also, a transformation of a new local reference system will give us more precise results in GPS time series.

5. Conclusions

In this study, the focal mechanisms of small earthquakes, west of Lefkas to North Cephalonia, are mainly characterized by horizontal slip faults. Specifically, as demonstrated by the method, the right-hand horizontal shift fault west of Cephalonia receives an address ~40° north, while for the department west of Lefkas, it turned out that the fault has a direction of 20° north. Also, the study of focal mechanisms indicates that west of Lefkas, the activation of a strike-slip fault occurred. East of Zakynthos up to the western part of the Peloponnese is predominated by horizontal sliding mechanisms, while in Zakynthos's bay, they respond mainly with reverse focal mechanisms. Most of the earthquakes in the area are associated with one right-hand horizontal slip. There are surface earthquakes with activation in the eastern part of the Ionian, mainly horizontal slip faults. Finally, in the southern part, inverted types of generating mechanisms are activated. The depth of the earthquakes studied in this area is between 12 and 30 km, which shows that they are increased compared to the usual depths are identified for surface earthquakes throughout Greece. Here the seismicity seems to be deeper than in other parts of Greece.

In the western part of Cephalonia Island, Ionian Sea, at the SSW-wards continuation of the Lefkas segment of the Cephalonia Transform Fault Zone (CTFZ), more than 8000 earthquakes occurred in the first year. The obtained results provided insights on the rupture mechanism and temporal distribution of the seismic sequence. Source parameters that are focal depth, fault plane solution, and seismic moment were determined by applying the moment tensor inversion methodology using regional data in distances less than 3°. The determined fault plane solutions represent a strike-slip fault's activation, and the depth distribution of the entire sequence ranges between 10 and 20 km. For the same region and events, the GNSS data were used and analyzed. The results indicate that an N–S displacement of ~7 mm and an E–W displacement of ~8 mm took place at station VLSM, and also at earthquake 3 February 2014 (03:08:44, UTC) M_L = 5.7 an N–S displacement of ~11.2 mm and E–W displacement ~8 mm took place at the same station and none of the other two stations were significantly affected. The seismic sequence of Cephalonia in

2014 is evolving into a seismic area with a general direction from NW to NN. The seismic sequence of Cephalonia in 2014 is evolving into a seismic area with a general direction from NW to NN and which is the continuation to the NN of the seismogenic area of Lefkas in 2003.

The second seismic sequence analyzed is the Lefkas Island earthquake (17 November 2015, 07:10:07, UTC) to the southwestern part of Lefkas island. In total, 2804 events that followed this event were recorded and analyzed to have a distribution of the epicenters. The moment tensor solution indicated the activation of a strike-slip fault with a right-lateral direction. The GNSS data analysis showed an N–S displacement of ~196 mm, an E–W displacement of ~374 mm, and a vertical displacement of ~58 mm at station PONT. From the analysis of the PONT station's geodetic data and the seismological waveforms' processing, it was observed that in the earthquake of 17 November 2015, the ruptured zone was broken, and not activated in the earthquake of 14 August 2003. Also, an N–S displacement of ~72 mm and E–W displacement of ~57.46 mm occurred at station SPAN; accordingly, an S–N displacement of ~6 mm and E–W displacement of ~18 mm took place at station VLSM. These results are confirmed by the focal mechanism that has already been calculated in the present study. We conclude that in Lefkada's earthquake, the seismic fault moved parallel to Lefkada's west coast in Cephalonia's direction. This is confirmed by the seismicity distribution that was presented in Figures 3 and 7b and the GNSS data processing. Finally, the earthquake sequence at the southern coast of Zakynthos Island that lasted from October 2018 April until the end of 2019 saw that this shallow event was followed by a rich aftershock sequence with a direction SW of the Zakynthos Island. In total, more than 12,000 events were recorded and analyzed in order to calculate the epicenter and the depth. The largest aftershocks of the sequence data were collected and processed to calculate the focal mechanism; the source parameters are the fault plane solution, the focal depth, and the moment magnitude. This analysis emerged for most of them the activation of a strike-slip fault for earthquakes with a focal depth of less than 10 km, while for those with a focal depth greater than 10 km, the activation of a thrust type faulting, with a component of strike-slip, indicates that the 25 October 2018 M_w = 6.7 event ruptured the Hellenic megathrust. This event highlights the high degree of seismic coupling in the Hellenic Arc western region. The GNSS data also point to a similar pattern between the coseismic strain released during 2014 until the end of the 2019 event and the long-term (interseismic) strain accumulation along the west Hellenic Arc. Also, the fault-plane geometry is well constrained by GNSS; this is consistent with the distribution of the aftershocks.

Author Contributions: A.M.: conceptualization, software, methodology, writing—original draft, writing—review and editing, Supervision, funding acquisition, investigation, visualization. P.A.: software, writing—original draft, writing—review and editing. A.K.: data curation, formal analysis, writing—original draft, writing—review and editing. A.-C.D.: data curation, software, visualization. N.C.S.: software, investigation, visualization. All authors have read and agreed to the published version of the manuscript.

Conflicts of Interest: The authors declare no conflict of interest.

Appendix A

Table A1. Source Parameters of the main events as well as for the intermediate magnitudes for Cephalonia Seismic Sequence for the period 2014–2019. Nr is the event number. Lat and Lon are the geographical coordinates of each event, as calculated by the National Observatory of Athens; M0 is the seismic Moment in dyn*cm, Mw is the moment magnitude; Strike, Dip, Rake of the two nodal planes are the seismic parameters as calculated from the inversion; CLVD is the percentage of the Compensated Linear Vector Dipole, which describes seismic sources with no volume changes; Nr of stations is the number of stations used in inversion and finally the quality of the solution depending on the misfit and the percentage CLVD.

Nr	Origin Date	Time	Location Lat (°)	Lon (°)	Mo (dyn·cm)	M_w	Depth (km) Catalog	MT	Plane 1 Strike (°)	Dip (°)	Rake (°)	Plane 2 Strike (°)	Dip (°)	Rake (°)	CLVD (%)	Nr of Stations	Quality
1	01/26/2014	13:55:42	38.2190	20.5320	1.510×10^{25}	6.1	21.1	13	23	68	175	115	85	22	3	5	A1
2	01/26/2014	14:08:39	38.1880	20.5325	2.960×10^{22}	4.3	18.9	12	20	64	170	114	81	26	15	4	B1
3	01/26/2014	14:21:58	38.2088	20.3787	9.520×10^{21}	4.0	9.9	8	22	67	168	117	79	23	12	4	C1
4	01/26/2014	14:24:04	38.2532	20.3903	2.220×10^{22}	4.2	14.5	14	19	62	170	114	81	28	16	4	B1
5	01/26/2014	14:41:39	38.2167	20.4757	2.220×10^{22}	4.2	17.1	13	20	60	172	114	83	30	13	4	B1
6	01/26/2014	14:55:50	38.2132	20.4100	9.520×10^{21}	4.0	14.2	14	23	68	176	115	86	22	12	4	B1
7	01/26/2014	14:59:25	38.3030	20.4753	7.350×10^{22}	4.5	12.9	12	25	65	179	115	89	25	10	4	B1
8	01/26/2014	15:36:39	38.2363	20.4373	1.380×10^{22}	4.1	17.1	13	18	64	170	112	81	26	8	5	C1
9	01/26/2014	18:45:08	38.2358	20.4410	5.990×10^{23}	5.2	16.5	20	19	62	170	114	81	28	9	5	A1
10	01/26/2014	19:03:07	38.1873	20.4177	2.960×10^{22}	4.3	17.1	13	20	69	169	114	80	21	12	5	A2
11	01/26/2014	19:12:04	38.2408	20.4002	4.060×10^{22}	4.4	18.0	12	22	70	168	116	79	20	15	4	A1
12	01/26/2014	21:15:34	38.1337	20.3002	8.170×10^{22}	4.6	10.4	11	23	65	170	117	81	25	14	4	B1
13	01/26/2014	21:42:12	38.1890	20.4862	9.520×10^{21}	4.0	13.0	13	17	64	165	114	77	27	13	4	B1
14	01/26/2014	23:06:55	38.2398	20.4297	2.220×10^{22}	4.2	18.3	13	24	65	174	117	85	25	12	4	A2
15	01/27/2014	9:47:38	38.1517	20.4025	1.380×10^{22}	4.1	14.8	14	26	68	175	118	85	22	10	4	A1
16	01/27/2014	13:05:50	38.2308	20.4403	2.960×10^{22}	4.3	11.1	11	19	69	169	113	80	21	8	4	B1
17	01/27/2014	15:39:34	38.3748	20.4222	2.220×10^{22}	4.2	13.8	13	20	80	173	289	83	10	7	4	C1
18	01/28/2014	1:05:55	38.2542	20.4347	9.520×10^{21}	4.0	15.1	12	20	65	172	113	83	25	12	4	B1
19	01/28/2014	5:12:53	38.2083	20.3817	2.960×10^{22}	4.3	12.8	8	22	62	170	117	81	28	8	4	C1
20	01/28/2014	8:07:11	38.2138	20.5502	9.520×10^{21}	4.0	15.3	11	23	60	172	117	83	30	13	4	A1
21	01/28/2014	14:49:33	38.2120	20.4552	9.520×10^{21}	4.0	17.7	11	25	68	174	117	84	22	10	4	B1
22	01/28/2014	19:12:11	38.4048	20.5022	1.380×10^{22}	4.1	10.6	12	17	64	176	109	86	26	12	4	A2
23	01/28/2014	22:22:37	38.4037	20.4885	2.220×10^{22}	4.2	15.6	13	20	65	173	113	84	25	9	4	A2
24	01/28/2014	22:23:39	38.3927	20.4418	2.220×10^{22}	4.2	15.9	12	22	60	175	115	86	30	13	4	B1
25	01/30/2014	11:06:18	38.4050	20.5267	4.060×10^{22}	4.4	9.2	8	4	73	159	100	70	18	12	4	C1
26	01/31/2014	6:52:47	38.4210	20.4843	4.060×10^{22}	4.4	12.4	12	19	64	170	113	81	26	7	4	B1
27	01/31/2014	12:45:40	38.4180	20.4677	2.960×10^{22}	4.3	18.6	13	18	65	170	112	81	25	12	4	A1
28	02/01/2014	16:33:38	38.1727	20.3876	7.350×10^{22}	4.5	10.6	12	17	68	175	109	85	22	8	4	B1
29	03/02/2014	3:08:44	38.2527	20.3948	2.460×10^{24}	6.0	10.5	17	20	67	174	112	84	23	10	5	A1
30	02/04/2014	19:42:12	38.2817	20.3702	2.220×10^{22}	4.2	16.5	11	23	66	172	116	83	24	10	4	B1
31	02/07/2014	3:26:43	38.3253	20.4325	2.220×10^{22}	4.2	13.0	9	25	60	170	120	81	30	12	4	A2
32	02/07/2014	8:59:43	38.2338	20.4558	2.220×10^{22}	4.2	12.9	12	20	65	175	114	81	25	9	4	B1
33	02/09/2014	8:22:58	38.1752	20.3675	7.350×10^{22}	4.5	11.2	12	20	67	180	110	90	23	12	4	B1

Table A1. *Cont.*

Nr	Origin		Location		Mo	M_w	Depth (km)		Plane 1			Plane 2			CLVD (%)	Nr of Stations	Quality
	Date	Time	Lat (°)	Lon (°)	(dyn·cm)		Catalog	MT	Strike (°)	Dip (°)	Rake (°)	Strike (°)	Dip (°)	Rake (°)			
34	02/12/2014	10:34:31	38.1655	20.3538	8.170×10^{22}	4.6	11.1	12	25	70	166	120	77	21	14	5	B1
35	02/14/2014	3:38:33	38.1677	20.3432	8.170×10^{22}	4.7	9.8	13	20	67	170	114	81	23	13	5	B1
36	02/21/2014	15:18:23	38.2147	20.9720	7.350×10^{22}	4.5	16.2	13	26	73	177	117	87	17	10	4	B1
37	03/05/2014	12:49:20	38.0780	20.3092	8.170×10^{22}	4.6	20.4	12	30	70	170	123	80	15	12	4	A1
38	03/05/2014	15:08:43	38.0792	20.3467	1.380×10^{22}	4.1	18.0	14	18	70	168	112	79	20	13	4	B1
39	03/05/2014	18:42:02	38.1423	20.4185	9.520×10^{21}	4.0	16.3	12	22	65	168	117	79	25	10	4	B1
40	03/10/2014	23:27:48	38.2087	20.2852	9.520×10^{21}	4.0	13.4	12	25	70	170	120	85	26	9	4	B1
41	11/05/2014	14:22:24	38.1027	20.4877	1.380×10^{22}	4.1	16.6	10	23	68	175	115	85	22	8	4	A1
42	11/07/2014	7:41:38	38.1020	20.4358	8.170×10^{22}	4.7	17.7	9	20	64	170	114	81	26	9	4	B1
43	11/08/2014	23:15:42	38.0998	20.4400	4.065×10^{25}	5.0	18.4	11	22	67	168	117	79	23	10	5	C1
44	11/12/2014	6:31:37	38.2893	20.4722	9.520×10^{21}	4.0	13.8	9	19	62	170	114	81	28	8	4	B1
45	11/13/2014	9:37:53	38.3803	20.5142	2.960×10^{22}	4.3	12.4	13	23	60	172	117	83	30	7	4	A1
46	11/24/2014	7:20:32	38.3022	20.3630	1.380×10^{22}	4.1	15.2	13	17	68	175	109	85	22	12	4	B1
47	12/11/2014	22:24:22	38.3815	20.4412	8.170×10^{22}	4.6	28.0	12	25	60	170	120	81	30	8	4	B1
48	03/31/2015	15:48:41	38.3173	20.5220	8.170×10^{22}	4.6	11.3	14	18	64	170	112	81	26	13	4	A2
49	04/04/2015	4:38:19	38.3108	20.5308	4.060×10^{22}	4.4	13.4	12	19	62	170	114	81	28	10	4	B1
50	06/02/2015	14:04:21	38.1465	20.4722	4.060×10^{22}	4.4	15.3	12	20	69	169	114	80	21	9	5	A1
51	11/17/2015	11:49:45	38.4862	20.4857	9.520×10^{21}	4.0	7.5	13	22	70	168	116	79	20	7	5	A2
52	11/18/2015	5:18:13	38.4967	20.5177	4.060×10^{22}	4.4	13.6	12	20	77	173	112	83	13	8	5	B1
53	11/19/2015	17:45:55	38.4623	20.4952	2.960×10^{22}	4.3	12.5	8	40	68	176	132	86	22	9	4	B1
54	11/20/2015	5:12:24	38.4703	20.4875	8.170×10^{22}	4.7	12.4	14	20	64	178	111	88	26	12	4	A1
55	01/04/2016	7:21:45	38.3155	20.4012	2.960×10^{22}	4.3	15.0	13	20	88	166	111	76	2	12	4	A2
56	04/11/2016	18:53:44	38.2133	20.3325	1.380×10^{22}	4.1	20.5	12	15	87	144	107	54	4	13	4	A1
57	15/01/2019	1:11:49	38.2898	20.4142	2.220×10^{22}	4.2	11.2	11	4	73	159	100	70	18	8	4	A1

Table A2. Source parameters of the main events and the intermediate magnitudes for Lefkas Seismic Sequence for the period 2015–2019. Nr is the event number. Lat and Lon are the geographical coordinates of each event, as calculated by the National Observatory of Athens; M_0 is the seismic moment in dyn*cm, M_w is the moment magnitude; Strike, Dip, Rake of the two nodal planes are the seismic parameters as calculated from the inversion; CLVD is the percentage of Compensated Linear Vector Dipole, which describes seismic sources with no volume changes; Nr of stations is the number of stations used in inversion and finally the quality of the solution depending from the misfit and the percentage CLVD.

Nr.	Origin		Location		M_0 (dyn*cm)	M_w	Depth (km)		Plane 1			Plane 2			CLVD (%)	Nr of Stations	Quality
	Date	Time	Lat (°)	Lon (°)			Catalog	MT	Strike (°)	Dip (°)	Rake (°)	Strike (°)	Dip (°)	Rake (°)			
1	11/17/2015	7:10:07	38.6655	20.6002	4.402×10^{28}	6.4	10.7	10	290	88	−12	20	82	−178	15	6	A1
2	11/17/2015	8:33:40	38.6515	20.5570	4.065×10^{25}	5.0	8.7	8	112	87	6	22	84	177	8	6	A1
3	11/17/2015	11:49:45	38.4862	20.4857	1.439×10^{22}	4.0	7.5	2	310	25	−8	43	83	−123	10	4	B1
4	11/17/2015	11:57:25	38.7025	20.6145	6.133×10^{22}	4.5	9.9	4	24	65	172	117	83	25	12	5	A2
5	11/17/2015	12:37:56	38.7022	20.6538	1.300×10^{23}	4.7	4.8	4	144	89	14	53	76	179	7	4	A1
6	11/17/2015	19:39:34	38.7040	20.6017	2.240×10^{22}	4.2	8.5	4	308	85	4	41	86	−175	10	4	A1
7	11/18/2015	5:18:13	38.4967	20.5177	5.817×10^{22}	4.4	13.6	8	336	86	172	67	81	9	9	5	A2
8	11/18/2015	12:15:38	38.8443	20.5915	3.857×10^{23}	5.0	17.2	10	203	71	−174	111	84	−19	6	5	A1
9	11/18/2015	13:03:14	38.7197	20.6288	1.483×10^{23}	4.7	8.3	4	314	96	−24	53	67	−158	5	5	A1
10	11/18/2015	18:30:07	38.7238	20.6280	2.443×10^{22}	4.2	6.3	2	290	86	155	21	59	7	10	4	A2
11	11/20/2015	5:12:24	38.4703	20.4875	1.746×10^{23}	4.8	12.4	8	116	80	5	26	85	170	6	5	A1
12	11/20/2015	9:33:14	38.6347	20.5830	7.662×10^{22}	4.5	10.7	6	203	80	175	294	85	10	7	5	A1
13	11/20/2015	23:37:04	38.7128	20.6093	9.104×10^{25}	4.6	12.0	2	302	57	−10	37	81	−146	9	4	A1
14	11/21/2015	0:41:56	38.7148	20.6170	7.199×10^{22}	4.5	9.3	2	297	80	−20	31	69	−168	10	4	A1
15	01/04/2016	18:00:55	38.6037	20.5917	2.720×10^{22}	4.2	14.1	10	29	47	−174	295	86	−43	10	4	A2
16	12/25/2017	23:47:05	38.5937	20.5613	5.817×10^{22}	4.4	4.7	8	111	70	50	357	52	150	7	4	A1
17	01/15/2019	1:25:05	38.9428	20.6178	5.817×10^{22}	4.4	18.8	11	119	58	30	14	71	150	5	4	A1
18	02/05/2019	2:26:09	38.9803	20.5870	4.065×10^{25}	5.0	13.2	10	224	27	170	317	85	54	6	5	A1
19	02/26/2019	10:05:59	38.8623	20.6104	1.439×10^{22}	4.0	4.6	8	291	53	−9	27	83	−142	10	4	A1

Table A3. Source parameters of the main events and the intermediate magnitudes for Zakynthos Seismic Sequence for the period 2018–2019. Nr is the event number. Lat and Lon are the geographical coordinates of each event, as calculated by the National Observatory of Athens; M_0 is the seismic moment in dyn*cm, Mw is the moment magnitude; Strike, Dip, Rake of the two nodal planes are the seismic parameters as calculated from the inversion; CLVD is the percentage of Compensated Linear Vector Dipole, which describes seismic sources with no volume changes; Nr of stations is the number of stations used in inversion and finally the quality of the solution depending from the misfit and the percentage CLVD.

Nr	Origin		Location		M_0 (dyn*cm)	M_w	Depth (km)		Plane 1			Plane 2			CLVD (%)	Nr of Stations	Quality
	Date	Time	Lat (°)	Lon (°)			Catalog	MT	Strike (°)	Dip (°)	Rake (°)	Strike (°)	Dip (°)	Rake (°)			
1	10/25/2018	22:22:53	37.3482	20.5547	1.746×10^{23}	4.8	5.0	15	140	70	80	347	22	116	10	4	A1
2	10/25/2018	22:54:50	37.3516	20.4922	1.450×10^{26}	6.7	12.8	17	123	42	30	10	70	128	20	5	A2
3	10/26/2018	5:48:36	37.3592	20.5058	4.065×10^{25}	5.0	3.1	16	19	39	139	143	66	59	12	5	A1
4	10/26/2018	1:06:03	37.3887	20.8560	7.350×10^{22}	4.5	5.6	15	33	47	170	130	83	43	15	4	A2
5	10/26/2018	0:13:39	37.4660	20.6712	7.350×10^{22}	4.5	5.7	18	19	28	176	113	88	62	13	4	A1
6	10/26/2018	12:41:13	37.3753	20.5360	5.420×10^{22}	5.1	7.3	19	23	28	163	128	82	63	8	4	A1
7	10/26/2018	16:07:09	37.4248	20.5892	4.060×10^{22}	4.4	6.7	15	341	56	140	69	57	41	10	5	A2
8	10/27/2018	5:28:46	37.4743	20.6392	4.060×10^{22}	4.4	5.1	12	25	61	126	149	45	44	12	4	A1
9	10/30/2018	2:59:59	37.5938	20.5123	5.820×10^{24}	5.4	6.9	18	36	41	152	148	72	53	7	4	A1
10	10/30/2018	8:32:26	37.4840	20.4300	1.746×10^{23}	4.8	11.3	17	124	81	77	360	16	145	10	5	A1
11	10/30/2018	15:12:02	37.4575	20.4522	1.900×10^{23}	5.8	5.5	19	18	28	164	122	83	63	5	5	A1
12	11/01/2018	2:44:48	37.3673	20.5658	8.170×10^{22}	4.6	11.3	18	20	25	166	123	84	66	13	4	A1
13	11/04/2018	3:12:44	37.3785	20.4113	1.746×10^{23}	4.8	5.2	17	16	28	166	119	84	66	9	5	A1
14	11/05/2018	6:46:12	37.6268	20.4863	7.350×10^{22}	4.5	8.3	17	10	24	179	101	90	66	10	4	A1
15	11/11/2018	23:38:35	37.6327	20.5055	1.746×10^{23}	4.8	7.0	18	12	27	178	104	89	63	12	5	A1
16	11/15/2018	9:02:05	37.5227	20.6825	1.746×10^{23}	4.8	17.4	15	22	29	156	133	79	63	12	5	A1
17	11/15/2018	9:09:26	37.4887	20.6503	7.350×10^{22}	4.5	6.8	17	42	49	167	141	80	42	10	4	A2
18	12/25/2018	1:41:27	37.3243	20.7963	8.170×10^{22}	4.6	12.3	14	14	25	168	115	85	66	10	4	A2

References

1. Lekkas, E.; Danamos, G.; Mavrikas, G. Geological Structure and Evolution of Kefallonia and Ithaki islands. *Bull. Geol. Soc. Greece* **2001**, *34*, 11–17. [CrossRef]
2. Stiros, S.C.; Pirazzoli, P.A.; Laborel, J.; Laborel-Deguen, F. The 1953 earthquake in Kefallinia (Western Hellenic Arc): Coastal uplift and halotectonic faulting. *Geophys. J. Int.* **1994**, *117*, 834–849. [CrossRef]
3. Louvari, E.; Kiratzi, A.A.; Papazachos, B.C. The Kefallinia transform fault and its extension to western Lefkas Island (Greece). *Tectonophysics* **1999**, *308*, 223–236. [CrossRef]
4. Finetti, I.; Morreli, C. Geophysical exprolation of the 44Mediterranean Sea. *Boll. Geofis. Teor.* **1973**, *15*, 263–341.
5. Stride, A.; Belderson, R.; Kenyon, N. Evolving miogeoanticlines of the Eastern Mediterranean (Hellenic, Calabrian and Cyprus outer ridges). *Philos. Trans. R. Soc. Lond.* **1979**, *282*, 255–285.
6. Finetti, I. Structure, stratigraphy and evolution of central Mediterranean. *Boll. Geofis. Teor. Appl.* **1982**, *24*, 247–426.
7. BP (British Petroleum) Co., Ltd. *The Geological Results of Petroleum Exploration in Western Greece: Institute for Geology and Subsurface Research (Now Institute of Geology and Mineral Exploration) Special Report 10*; BP (British Petroleum) Co., Ltd.: London, UK, 1971; pp. 1–73.
8. Mercier, J.; Bousquet, B.; Delibassis, N.; Drakopoulos, I.; Keraudren, B.; Lemeille, F.; Sorel, D. Deformations en compression dans le Quaternaire des rivages ionien, Donnes neotectoniques et seismiques. *C. R. Acad. Sci. Paris* **1972**, *275*, 2307–2310.
9. Cushing, M. Evolution Structural de la Marge Nord-Ouest Hellenique Dans l" Ile de Lefkas et Ses Environs (Grece Nord-Occidentale). Ph.D. Thesis, Univ. d"Orsay, Paris, France, 1985.
10. Scordilis, E.M.; Karakaisis, G.F.; Karakostas, B.G.; Panagiotopoulos, D.G.; Comninakis, P.E.; Papazachos, B.C. Evidence for transform faulting in the Ionian Sea: The Kefallinia island earthquake sequence of 1983. *Pure Appl. Geophys.* **1985**, *123*, 388–397. [CrossRef]
11. Anderson, H.; Jackson, J. Active tectonics of the Adriatic region. *Geophys. J. Int.* **1987**, *91*, 937–983. [CrossRef]
12. Jackson, J.; McKenzie, D. The relationship between plate motions and seismic moment tensors, and the rates of active deformation in the Mediterranean and Middle East. *Geophys. J. Int.* **1988**, *93*, 45–73. [CrossRef]
13. Kiratzi, A.A.; Langston, C.A. Moment tensor inversion of the 1983 17 January Kefallinia event of Ionian Islands (Greece). *Geophys. J. Int.* **1991**, *105*, 529–535. [CrossRef]
14. Hatzfeld, D.; Kassaras, I.; Panagiotopoulos, D.; Amorese, D.; Makropoulos, K.; Karakaisis, D.; Coutant, O. Microseismicity and strain pattern in northwestern Greece. *Tectonics* **1995**, *14*, 773–785. [CrossRef]
15. Kahle, H.; Muller, M.; Geiger, A.; Danuser, G.; Mueller, S.; Veis, G.; Billiris, H.; Paradissis, D. The strain field in northwestern Greece and the Ionian islands: Results inferres from G.P.S. measurements. *Tectonophysics* **1995**, *249*, 41–52. [CrossRef]
16. Kahle, H.; Muller, M.; Veis, G. Trajectories of crustal deformation of Western Greece fromGPS observations 1989–1994. *J. Geophys. Lett.* **1996**, *23*, 677–680. [CrossRef]
17. Makropoulos, K.; Diagourtas, D.; Kassaras, J.; Kouskouna, V.; Papadimitriou, P.; Ziazia, M. The November–December 1994 Lefkas (W. Greece) earthquake sequence: Results from in situ seismological survey (abstract). In Proceedings of the 1st Congress of the Balkan Geophysical Society, Athens, Greece, 23–27 September 1996.
18. Sachpazi, M.; Hirn, A.; Laigle, M.C.; Haslinger, F.; Kissling, E.; Hello, Y.C.; Lépine, J.C.; Sapin, M.; Ansorge, J. Western Hellenic subduction and Kefallinia Transform: Local earthquakes and plate transport and strain. *Tectonophysics* **2000**, *319*, 301–319. [CrossRef]
19. Konstantaras, A. Expert knowledge-based algorithm for the dynamic discrimination of interactive natural clusters. *Earth Sci. Inf.* **2016**, *9*, 95–100. [CrossRef]
20. Konstantaras, A. Classification of distinct seismic regions and regional temporal modelling of seismicity in the vicinity of the Hellenic seismic arc. *IEEE J. Sel. Top. Appl. Earth Obs. Remote Sens.* **2013**, *6*, 1857–1863. [CrossRef]
21. Konstantaras, A.; Vallianatos, F.; Varley, M.R.; Makris, J.P. Soft-computing modelling of seismicity in the southern Hellenic Arc. *IEEE Geosci. Remote Sens. Lett.* **2008**, *5*, 323–327. [CrossRef]
22. Konstantaras, A. Deep Learning and Parallel Processing Spatio-Temporal Clustering Unveil New Ionian Distinct Seismic Zone. *Informatics* **2020**, *7*, 39. [CrossRef]
23. Emodnet-bathymetry.eu. Emodnet Bathymetry. 2021. Available online: https://www.emodnet-bathymetry.eu (accessed on 18 January 2021).
24. EU-DEM. 2021. Available online: https://land.copernicus.eu/imagery-in-situ/eu-dem (accessed on 18 January 2021).
25. Basili, R.; Kastelic, V.; Demircioglu, M.B.; Moreno, D.G.; Nemser, E.S.; Petricca, P.; Sboras, S.P.; Besana-Ostman, G.M.; Cabral, J.; Camelbeeck, T.; et al. The European Database of Seismogenic Faults (EDSF) Compiled in the Framework of the Project SHARE. 2013. Available online: http://diss.rm.ingv.it/share-edsf/ (accessed on 18 January 2021). [CrossRef]
26. Moshou, A. Strong earthquake sequences in Greece during 2008–2014: Moment Tensor inversions and fault plane discrimination. *Open J. Earthq. Res.* **2020**, *9*, 323–348. [CrossRef]
27. Bbnet.gein.noa.gr. NOA Seismic Network (HL)—Introduction. 2021. Available online: https://bbnet.gein.noa.gr/HL (accessed on 18 January 2021).

28. Geophysics.geol.uoa.gr. Department of Geophysics—Geothermics. 2021. Available online: http://www.geophysics.geol.uoa.gr (accessed on 18 January 2021).

29. Geophysics.geo.auth.gr. Τομέας Γεωφυσικής Α.Π.Θ. 2021. Available online: http://geophysics.geo.auth.gr (accessed on 18 January 2021).

30. Seismo.geology.upatras.gr. UPSL—Uni. Patras Seismological Laboratory. 2021. Available online: http://seismo.geology.upatras.gr (accessed on 18 January 2021).

31. Gein.noa.gr. Noanet Greece Gnss Network. 2021. Available online: http://www.gein.noa.gr/services/GPS/noa_gps.html (accessed on 18 January 2021).

32. Estey, L.H.; Meertens, C.M. TEQC: The Multi-Purpose Toolkit for GPS/GLONASS Data. *GPS Solut.* **1999**, *3*, 42–49. [CrossRef]

33. Ganas, A.; Karastathis, V.; Moshou, A.; Valkaniotis, S.; Mouzakiotis, E.; Papathanassiou, G. Aftershock relocation and frequency–size distribution, stress inversion and seismotectonic setting of the 7 August 2013 M = 5.4 earthquake in Kallidromon Mountain, central Greece. *Tectonophysics* **2014**, *617*, 101–113. [CrossRef]

34. Ganas, A.; Kourkouli, P.; Briole, P.; Moshou, A.; Elias, P.; Parcharidis, I. Coseismic Displacements from Moderate-Size Earthquakes Mapped by Sentinel-1 Differential Interferometry: The Case of February 2017 Gulpinar Earthquake Sequence (Biga Peninsula, Turkey). *Remote Sens.* **2017**, *10*, 1089. [CrossRef]

35. Randal, G.E. Efficient calculation of complete differential seismograms for laterally homogeneous earth models. *Geophys. J. Int.* **1994**, *118*, 245–254. [CrossRef]

36. Kennett, B.N.L. *Seismic Wave Propagation in Stratified Media*; Cambridge University Press: Cambridge, UK, 1983.

37. Haslinger, F.; Kissling, E.; Ansorge, J.; Hatzfeld, D.; Papadimitriou, E.; Karakostas, V.; Makropoulos, K.; Kahl, H.G.; Peter, Y. 3D crustal structure from local earthquake tomography around the Gulf of Arta (Ionian region, N.W. Greece). *Tectonophysics* **1999**, *304*, 201–218. [CrossRef]

38. Konstantinou, K.; Melis, N.; Boukouras, K. Routine Regional Moment Tensor Inversion for Earthquakes in the Greek Region: The National Observatory of Athens (N.O.A.) Database (2001–2006). *Seismol. Res. Lett.* **2010**, *81*, 750–760. [CrossRef]

39. Melis, N.; Konstantinou, K. Real-time Seismic Monitoring in the Greek Region: An Example from the 17 October 2005 East Aegean Sea Earthquake Sequence. *Seismol. Res. Lett.* **2006**, *77*, 364–370. [CrossRef]

40. Maravelakis, E.; Konstantaras, A.; Kabassi, K.; Chrysakis, I.; Georgis, C.; Axaridou, A. 3DSYSTEK web-based point cloud viewer. In Proceedings of the 5th International Conference on Information, Intelligence, Systems & Applications (IISA 2014), Chania, Greece, 7–9 July 2014; pp. 262–266.

41. Axaridou, A.; Chrysakis, I.; Georgis, C.; Theodoridou, M.; Doerr, M.; Konstantaras, A.; Maravelakis, E. 3D-SYSTEK: Recording and exploiting the production workflow of 3D-models in cultural heritage. In Proceedings of the 5th International Conference on Information, Intelligence, Systems & Applications (IISA 2014), Chania, Greece, 7–9 July 2014; pp. 51–56.

42. Karastathis, V.; Koukouvelas, I.; Ganas, A.; Moshou, A.; Mouzakiotis, A.; Papadopoulos, G.; Spanos, A. The strong Mw6 earthquake of 26 January 2014 in Kefallinia island, Ionian Sea, Greece: A first report. In Proceedings of the European Geosciences Union General Assembly 2014, Vienna, Austria, 27 April–2 May 2014; Volume 16, p. E.G.U. 2014-1700.

43. Chouliaras, G.; Makropoulos, K.; Melis, N.; Drakatos, G.; Argyrakis, P.; Boukouras, K.; Petro, P.; European Seismological Commission. Improving the detecta bility of seismic events in Greece: The rapid deployment of N.O.A.'s portable seismographic network. In Proceedings of the European Seismological Commission 32nd General Assembly, Montpellier, France, 6–10 September 2010.

44. Chouliaras, G. The rapid deployment of portable seismographic networks for real-time earthquake hazard assessment. In Proceedings of the International Workshop on Seismic Hazard and Earthquake Engineering, Kefalonia, Greece, 24–25 September 2014.

45. Emsc-csem.org. Moment Tensors. 2021. Available online: https://www.emsc-csem.org/Earthquake/tensors.php?id=355461&year=2014 (accessed on 18 January 2021).

46. Papathanassiou, G.; Ganas, A.; Moshou, A.; Valkaniotis, S. Geoenviromental effects of the M = 6.4, 17 November 2015 earthquake on south Lefkas, Ionian Sea, Greece. *Bull. Geol. Soc. Greece* **2016**, *50*, 521–539. [CrossRef]

47. Papathanassiou, G.; Pavlides, S.; Ganas, A. The 2003 Lefkas earthquake: Field observations and preliminary microzonation map based on liquefaction potential index for the town of Lefkas. *Eng. Geol.* **2003**, *82*, 12–31. [CrossRef]

48. Papadopoulos, G.A.; Karastathis, V.K.; Ganas, A.; Pavlides, S.; Fokaefs, A.; Orfanogiannaki, K. The Lefkas, Ionian Sea (Greece), shock (Mw 6.2) of 14 August 2003: Evidence for the characteristic earthquake from seismicity and ground failures. *Earth Planets Space* **2003**, *55*, 713–718. [CrossRef]

49. Ganas, A.; Briole, P.; Papathanassiou, G.; Bozionelos, G.; Avallone, A.; Melgar, D.; Argyrakis, P.; Valkaniotis, S.; Mendonidis, E.; Moshou, A.; et al. A Preliminary Report on the 17 November, 2015 M = 6.4 South Lefkas Earthquake, Ionian Sea, Greece. Report on Emsc Csem. 2015. Available online: https://www.emsc-csem.org/Doc/Additional_Earthquake_Report/470390/Lefkas%2017%20Nov%202015%20earthquake%20report.pdf (accessed on 18 January 2021).

50. Karakostas, V.; Papadimitriou, E.; Papazachos, C. Properties of the 2003 Lefkada, Ionian Islands, Greece, Earthquake Seismic Sequence and Seismicity Triggering. *Bull. Seismol. Soc. Am.* **2003**, *94*, 1976–1981. [CrossRef]

51. Bbnet.gein.noa.gr. BBNET—Database of Revised Events (Since 01 January 2008). 2021. Available online: https://bbnet.gein.noa.gr/HL/databases/database (accessed on 18 January 2021).

52. Sokos, E.; Gallovič, F.; Evangelidis, C.P.; Serpetsidaki, A.; Plicka, V.; Kostelecký, J.; Zahradník, J. The 2018 Mw 6.8 Zande, Greece, earthquake: Dominant strike-slip faulting near subducting slab. *Seismol. Res. Lett.* **2020**, *91*, 721–732. [CrossRef]

53. Zahradnik, J.; Sokos, E.; Plicka, V. Zande 25 October 2018, Mw 6.8 Earthquake: Superposition of Strike-Slip and Thrust? EMSC Web Report. 2018. Available online: https://www.emsccsem.org/Files/news/Earthquakes_reports/Zande_2018_Report.pdf (accessed on 18 January 2021).

54. Ganas, A.; Briole, P.; Bozionelos, G.; Elias, P.; Valkaniotis, S.; Tsironi, V.; Moshou, A.; Andritsou, N. The 25 October, 2018 M6.7 Zande Earthquake Sequence (Ionian Sea, Greece): Fault Modelling from Seismic and GNSS Data and Implications for Seismic Strain Release Along the Western Hellenic Arc. *Bull. Geol. Soc. Greece* **2019**, *7*, 602–603.

55. Papadimitriou, P.; Chousianitis, K.; Agalos, A.; Moshou, A.; Lagios, E.; Makropoulos, K. The spatially extended 2006 April Zande (Ionian Islands, Greece) seismic sequence and evidence for stress transfer. *Geophys. J. Int.* **2012**, *190*, 1025–1040. [CrossRef]

56. Gipsy-oasis.jpl.nasa.gov. 2021. Available online: http://gipsy-oasis.jpl.nasa.gov (accessed on 18 January 2021).

57. Zumberge, J.F.; Heflin, M.B.; Jefferson, D.C.; Watkins, M.M.; Webb, F.H. Precise point positioning for the efficient and robust analysis of G.P.S. data from large network. *J. Geophys. Res.* **1997**, *102*, 5005–5017. [CrossRef]

58. Hill, E.M.; Blewitt, G. Testing for fault activity at Yucca Mountain, Nevada, using independent G.P.S. results from the BARGEN network. *Geophys. Res. Lett.* **2006**, *33*. [CrossRef]

59. Rozsa, S. Modelling Tropospheric Delays Using the Global Surface Meteorological Parameter Model GPT2. *Period Polytech. Civ. Eng.* **2014**, *58*, 301–308. [CrossRef]

60. Wang, M.; Li, B. Evaluation of Empirical Tropospheric Models Using Satellite-Tracking Tropospheric Wet Delays with Water Vapor Radiometer at Tongji, China. *Sensors* **2016**, *16*, 186. [CrossRef]

61. Steigenberger, P.; Boehm, J.; Tesmer, V. Comparison of GMF/GPT with VMF1/ECMWF and Implications for Atmospheric Loading. *J. Geod.* **2009**, *83*, 943. [CrossRef]

62. Igs.org. WG/PP Registration—International GNSS Service. Available online: http://www.igs.org/wg (accessed on 18 January 2021).

63. Wahr, J.M. Deformation induced by polar motion. *J. Geophys. Res.* **1995**, *90*, 9363–9368. [CrossRef]

64. Wu, D.; Yan, H.; Shen, Y. TSAnalyzer, a GNSS time series analysis software. *GPS Solut.* **2017**, *21*, 1389–1394. [CrossRef]

65. Papadopoulos, G.; Karastathis, V.; Koukouvelas, I.; Sachpazi, M.; Baskoutas, I.; Chouliaras, G.; Agalos, A.; Daskalaki, E.; Minadakis, G.; Moschou, A.; et al. The Kefallinia, Ionian Sea (Greece), sequence of strong earthquakes of January–February 2014: A first report. *Res. Geophys.* **2014**, *4*, 19–30.

66. Benetatos, C.; Kiratzi, A.; Roumelioti, Z.; Stavrakakis, G.; Drakatos, G.; Latoussakis, I. The 14 August 2003 Lefkas Island (Greece) earthquake: Focal mechanisms of the mainshock and of the aftershock sequence. *J. Seismol.* **2005**, *9*, 171–190. [CrossRef]

67. Parkinson, B.W.; Enge, P. Differential G.P.S. In *Global Positioning System: Theory and Applications*; Parkinson, B., Spilker, J., Axelrad, P., Enge, P., Eds.; American Institute of Aeronautics and Astronautics: Reston, VA, USA, 1996; Volume II, pp. 3–50.

68. Rebischung, P.; Altamimi, Z.; Ray, J.; Garayt, B. The IGS contribution to ITRF2014. *J. Geod.* **2016**, *90*, 611–630. [CrossRef]

69. Sakkas, V.; Lagios, E. Ground deformation effects from the M6 earthquakes (2014–2015) on Kefallinia–Ithaca Islands (Western Greece) deduced by G.P.S. observations. *Acta Geophys.* **2017**, *65*, 207–222. [CrossRef]

70. Chousianitis, K.; Konca, A.O.; Tselentis, G.-A.; Papadopoulos, G.A.; Gianniou, M. Slip model of the 17 November 2015 Mw = 6.5 Lefkada earthquake from the joint inversion of geodetic and seismic data. *Geophys. Res. Lett.* **2016**, *43*, 7973–7981. [CrossRef]

71. Avallone, A.; Cirella, A.; Cheloni, D.; Tolomei, C.; Theodoulidis, N.; Piatanesi, A.; Briole, P.; Ganas, A. Near-source high-rate G.P.S., strong motion and InSAR observations to image the 2015 Lefkada (Greece) Earthquake rupture history. *Sci. Rep.* **2017**, *7*, 10358. [CrossRef]